H. S. BRAHINSKY

SEP 28 1984

AEDC-TR-69-78

EXPERIMENTAL DETERMINATION OF GAS PROPERTIES AT HIGH TEMPERATURES AND/OR PRESSURES

C. Carey, E. H. Carnevale, S. Uva and T. Marshall

Panametrics, Inc.

Waltham, Massachusetts

March 1969

ARNOLD ENGINEERING DEVELOPMENT CENTER
AIR FORCE SYSTEMS COMMAND
ARNOLD AIR FORCE STATION, TENNESSEE

NOTICES

When U. S. Government drawings specifications, or other data are used for any purpose other than a definitely related Government procurement operation, the Government thereby incurs no responsibility nor any obligation whatsoever, and the fact that the Government may have formulated, furnished, or in any way supplied the said drawings, specifications, or other data, is not to be regarded by implication or otherwise, or in any manner licensing the holder or any other person or corporation, or conveying any rights or permission to manufacture, use, or sell any patented invention that may in any way be related thereto.

Qualified users may obtain copies of this report from the Defense Documentation Center.

References to named commercial products in this report are not to be considered in any sense as an endorsement of the product by the United States Air Force or the Government.

EXPERIMENTAL DETERMINATION OF GAS PROPERTIES AT HIGH TEMPERATURES AND/OR PRESSURES

C. Carey, E. H. Carnevale, S. Uva and T. Marshall
Panametrics, Inc.
Waltham, Massachusetts

FOREWORD

This report was prepared by Panametrics, Inc., Waltham, Massachusetts, under U. S. Air Force Contract No. AF 40(600)-1191. This contract was initiated under Air Force Project 8951, Task No. 895102, Program Element 61102F. The work was sponsored under the direction of Arnold Engineering Development Center, Air Force Systems Command, with Captain Terry L. Hershey, Project Manager.

This report covers work performed between September 1967 and October 1968.

The manuscript was released by the authors October 1968 for publication as a technical report.

The authors would like to acknowledge David Winslow and Charles Barber for performing measurements and Gerald Diebold for aid in data reduction and data review. The authors are grateful to Dr. Tunis Wentink, Jr. for reviewing the final manuscript.

This technical report has been reviewed and is approved.

Michael G. Buja
2nd Lt, USAF
Research Division
Directorate of Plans
and Technology

Edward R. Feicht
Colonel, USAF
Directorate of Plans
and Technology

ABSTRACT

The problem of extending transport property measurements to conditions of high pressure $p < 10^4$ atm and temperature $T < 20,000^{\circ}K$ beyond the range of conventional techniques is summarized. The advantages of unconventional techniques over conventional transport property measurement techniques in regions where they overlap are presented for application at extreme pressure-temperature conditions. The application of ultrasonic absorption and sound speed to the determination of thermodynamic and transport properties at high pressures is discussed. Measurements are presented at $300^{\circ}K$ and pressures up to 100 atm in the argon-nitrogen and helium-argon systems. The schlieren differential interferometer is applied to thermal conductivity measurements at high pressures and/or temperatures. Some thermal conductivity measurements in nitrogen and air are reported at temperatures between 2000 and $5000^{\circ}K$.

TABLE OF CONTENTS

LIST OF ILLUSTRATIONS

LIST OF SYMBOLS

λ	Thermal conductivity or wavelength of light
η	Viscosity or similarity parameter
η'	Bulk viscosity
D	Diffusion coefficient
σ	Effective hard sphere cross section for viscosity
χ	Enskog factor
a_T	Thermal diffusion factor
Z_{rot}	Number of collisions necessary for rotation to come into thermal equilibrium with translation $\frac{\tau}{\tau_c}$
τ	Relaxation time
τ_c	Collisional relaxation
ρ	Density
p	Pressure
T	Temperature
v	Mass average velocity
U	Internal energy
K_T	Isothermal compressibility
β	Thermal expansion coefficient
C_v	Specific heat at constant volume
C_p	Specific heat at constant pressure
C_i	Internal specific heat

LIST OF SYMBOLS (cont' d)

γ	Specific heat ratio $\frac{C_p}{C_v}$
z	Compressibility factor $p = \rho z R T$
c	Sound speed
α	Sound attenuation coefficient
β', β''	Weighted mass ratios Eq. (14)
ϕ	Phase shift radians
ℓ	Path length of test region
η	Index of refraction
d	Separation of rays
s	Fringe spacing (Δs fringe shift)
a	Gladstone-Dale constant, or piston radiator diameter
y	Distance from end wall

SECTION I

INTRODUCTION

Experiments described in the present report include ultrasonic measurements in the high pressure ($p < 400$ atm) region as well as schlieren interferometer measurements in the high temperature ($1000 < T < 5000^{\circ}K$) region. Ultrasonic measurement of sound absorption and velocity were made in nitrogen, argon, two mixtures of nitrogen and argon, and a 50-50 helium-argon mixture. The pressure of these measurements ranged up to 400 atm at $\sim 300^{\circ}K$. Schlieren interferometric measurements of thermal conductivity of nitrogen, air and a helium-argon mixture at temperatures up to $5000^{\circ}K$ and pressures about 1 atm were obtained. The experimental work was done to extend the information on transport properties needed for engineering design at high pressures and temperatures as well as for long range support of theoretical developments.

Over the past two years we have assessed the problem areas in transport properties of gases* and designed experimental techniques to provide data in these areas. The problem areas we have investigated are shown graphically in Figure 1 for air. Also shown are techniques, we feel, will provide useful data in their respective ranges. Higher order collisions at high densities, diffusion coefficients under conditions where reaction conductivity is important, and ionized gases, are the major problem areas we have covered. In addition, at low pressures (1 atm) and intermediate temperatures ($1000^{\circ}C$) there are questions (Refs. 3, 4) about the available viscosity measurements which are the major experimental inputs for the determination of accurate molecular potential functions. The potential functions are needed in engineering practice for the calculation of thermodynamic and transport properties.

The solid lines in Figure 1 show the P-T curve along which higher order collisions cause a 30% and 70% increase in thermal conductivity respectively over the low pressure values. Pressures above and temperatures below these lines result in density effects of even greater importance. The heat transfer measurement provides thermal conductivity and the ultrasonic measurements provide viscosity and thermodynamics (specific heat and compressibility). A third technique which uses schlieren interferometric determination of the temperature field about a heated or cooled cylinder to determine thermal

*We have not considered the important problems which arise near a phase change (Refs. 1, 2).

conductivity was also conceived for use at high pressures and temperatures. The end wall heat transfer and the interferometric method of determining thermal conductivity are not affected as much as the conventional techniques for high pressure applications by convection and radiation. The interferometric measurement is capable of operating at higher temperatures than conventional techniques. In addition, some questions have arisen about the validity of previous viscosity measurements which do not apply to the ultrasonic technique. Finally, thermodynamic properties (specific heat, compressibility) of the high pressure gas which are not always known accurately at the pressures and temperatures of interest are a by-product of the ultrasonic velocity measurement.

The pressure-temperature range where dissociation is important is indicated by the dotted lines. The thermal conductivity of a simple dissociating diatomic gas is discussed to illustrate the problems involved. The equilibrium thermal conductivity of such a dissociating gas is given by

$$\lambda = \lambda_f + \rho D (h_m - h_a) \frac{\partial \alpha}{\partial T}$$

where α is the degree of dissociation, h_m and h_a are the enthalpy of molecules and atoms, respectively, and λ_f is the thermal conductivity due to translational energy (frozen thermal conductivity), $\rho D (h_m - h_a) \frac{\partial \alpha}{\partial T}$ is the thermal conductivity due to diffusion of dissociated species to cooler regions with subsequent recombination (chemical thermal conductivity). The chemical thermal conductivity is up to 6 times the frozen thermal conductivity depending on the pressure and temperature as indicated in Figure 1. Examination of the scanty evidence available at high temperatures from the Maecker arc and the schlieren interferometer indicates minimum uncertainties (Ref. 7) of thermal conductivity of 50-100% near the 50% dissociation temperature in nitrogen and air. The thermodynamic quantities, ρ, h_a, h_m and $\frac{\partial \alpha}{\partial T}$ may be calculated accurately. Accepting an uncertainty in the diffusion coefficient (D) of 20% (as is often quoted in existing tabulations) the large enthalpy associated with dissociation (h_m-h_a) transforms the 20% uncertainty in the calculated diffusion coefficient directly into a 20% uncertainty in thermal conductivity. Accurate determination of the diffusion coefficients between 2000 and 8000°K is an immediate engineering need. The most serious need exists around 4000°K at pressures between 1/2-30 atm.

The techniques shown in Figure 1 for application in the dissociating region are schlieren interferometry and the ultrasonic technique. Schlieren interferometry has been used during the past year to measure equilibrium thermal conductivities of nitrogen, air and a helium-argon mixture at pressures between 0.1 and 1 atm and at temperatures about 4000°K. The ultrasonic technique may in some cases be used to obtain the frozen thermal conductivity. The chemical thermal conductivity and therefore the diffusion coefficients may in principal be obtained from a combination of the schlieren and ultrasonic techniques.

The high temperature range above 10,000°K has not been investigated under the present contract but it is one of the areas of major uncertainty. The transport properties of ionized gases between 0.1 and 100 atm are an engineering requirement for the development and use of high enthalpy test facilities. The techniques which have been successfully applied to this area are the Maecker arc technique (Refs. 5, 6, 7) and the ultrasonic technique (Refs. 8, 9, 10). Electrical conductivity measurements are also useful. The ultrasonic technique requires reaction rates for ionization and collision numbers for electronic excitation to obtain transport properties. The Maecker arc technique requires electrical conductivity and radiative properties of the gas to be known before the thermal conductivity can be determined. The schlieren interferometric technique on the end wall of the shock tube may be used to obtain $\frac{\lambda}{C_p}$ between 8000 and 15,000°K with no knowledge of other gas properties except the Gladstone-Dale constant (Refs. 11, 12, 13).

Summarizing, the methods discussed below include end wall heat transfer and ultrasonic absorption for high pressure transport property measurements. These experiments are complementary since end wall heat transfer provides thermal conductivity and ultrasonics provide viscosity and thermodynamics. A new experiment involving schlieren measurements of the density field about a horizontal cylinder in convective flow is mentioned to provide high density thermal conductivity at high temperatures ($T \sim 3000$°K). The schlieren interferometric measurement in the end wall boundary layer is also presented as a means of measuring equilibrium thermal conductivity in the low pressures, high temperatures region where chemical reactions are in progress. This measurement combined with ultrasonic measurements of frozen thermal conductivity provides the reaction conductivity. The reaction conductivity is the chief source of pressure dependence in chemically reacting gases (dissociating air) and is therefore an immediate engineering requirement. Finally, new measurements relating to conductivity, viscosity, diffusion coefficients and thermodynamic properties of several gases are presented.

SECTION II

THEORY OF ULTRASONIC ABSORPTION AT HIGH PRESSURES

2.1 CONSERVATION EQUATIONS AND EQUATIONS OF STATE

The ultrasonic method for determining transport properties of gas was used to determine the effects of density on the transport and thermodynamic properties of gases. The general range of application of the ultrasonic techniques (including Brillouin scattering) was discussed in last year's report (Ref. 7).

The present discussion provides working equations for ultrasonic absorption and dispersion which are valid at high densities ($\rho \leq 400$ atm). The usual expressions for sound absorption and velocity in low pressure gases have the density eliminated in favor of the pressure using the equation of state. However, density is the fundamental variable and is simpler to keep at high densities. The potential energy of a molecule in the field of its neighbors becomes an important contribution to the internal energy at high densities. This leads to the appearance of a term proportional to the excess density in the equation of state for the internal energy. However, the interaction of a molecule with its nearest neighbor is not sufficient to affect the rotational and vibrational (Ref. 14) relaxation times up to densities approaching liquid densities. The change in relaxation time which does occur is due to a change in collisional time rather than the transition probability. Finally, an additional effect which becomes important near liquid densities is a bulk viscosity due to higher order collisions.

The basic phenomena which govern the sound absorption and speed are conservation of

energy
$$\frac{\partial \tilde{U}}{\partial t} + \frac{p}{\rho}\frac{\partial \tilde{v}}{\partial x} - \frac{\lambda}{\rho}\frac{\partial^2 \tilde{T}}{\partial x^2} = 0 \tag{1}$$

momentum
$$\frac{\partial \tilde{v}}{\partial t} + \frac{1}{\rho}\frac{\partial \tilde{p}}{\partial x} - \frac{1}{\rho}\left(\eta' + \frac{4}{3}\eta\right)\frac{\partial^2 \tilde{v}}{\partial x^2} = 0 \tag{2}$$

mass
$$\frac{\partial \tilde{\rho}}{\partial t} + \rho\frac{\partial \tilde{v}}{\partial x} = 0 \tag{3}$$

and the equations of state for pressure

$$\frac{\tilde{\rho}}{\rho} = K_T \tilde{p} - \beta \tilde{T} \tag{4}$$

and internal energy $$\tilde{U} = \left(\frac{\partial U}{\partial T}\right)_\rho \tilde{T} + \left(\frac{\partial U}{\partial \rho}\right)_T \tilde{\rho} \tag{5}$$

where the tilde represents the fluctuating part of the dependent variables and the dependent variables are the internal energy U, temperature T, density ρ, pressure p, and velocity v. The linearized conservation equations are exact for typical sound waves because the fluctuation of temperature, pressure, and density in a typical sound wave are about 10^{-4} of the ambient values. The only assumptions involved in the equations of state are those for small departures from equilibrium, the isothermal compressibility K_T, thermal coefficient of expansion β; specific heat $C_v = (\partial U/\partial T)_\rho$, and $(\partial U/\partial \rho)_T$ are essentially the equilibrium properties of the gas.

2.2 SOUND SPEED AND SPECIFIC HEAT RATIO DETERMINATION

The assumption that the ultrasonic pulse may be made up of exponentially damped plane waves leads to an expression for the absorption coefficient α and sound speed c. The viscosity and thermal conductivity are set equal to zero in the sound speed calculation since they have a negligible effect on the sound speed in the continuum density range (Refs. 9, 10). The condition that Eqs. (1-5) have a plane wave solution gives

$$\frac{1}{c^2} = \frac{\rho K_T C_v}{C_v + \left[\frac{p}{\rho} - \rho \left(\frac{\partial U}{\partial \rho}\right)_T\right] \beta} \tag{6}$$

Using the thermodynamic identity

$$C_p - C_v = \left[\frac{p}{\rho} - \rho \left(\frac{\partial U}{\partial \rho}\right)_T\right] \beta \tag{7}$$

the sound speed becomes

$$c^2 = \frac{\gamma}{\rho K_T} \tag{8}$$

The sound speed measured as a function of both temperature and pressure is sufficient to determine all the thermodynamic properties of the gas (Ref. 7). However, in the present instance it is more valuable to use compressibility factors from p V T measurements to obtain the specific heat ratio γ. The sound speed in terms of the compressibility is

$$c^2 = \gamma z R T \left[1 - \frac{p}{z}\left(\frac{\partial z}{\partial p}\right)_T\right]^{-1} \tag{9}$$

Equation (9) is useful (as is described below) to obtain specific heat ratios for reducing sound absorption to thermal conductivity.

2.3 THERMAL CONDUCTIVITY AND VISCOSITY

The absorption due to thermal conductivity and viscosity referred to as the classical absorption a_c may be similarly derived from Eqs. (1-5) (Ref. 10). The resulting expression is

$$\frac{\rho a_c}{\omega^2} = \frac{1}{2}\,\frac{1}{c^3}\left[\frac{4}{3}\eta + \frac{\gamma - 1}{C_p}\lambda\right] \tag{10}$$

where ρ is the density, c sound speed, C_p specific heat, γ specific heat ratio, η viscosity and λ thermal conductivity. The viscosity and thermal conductivity terms increase with pressure. However, the sound speed cubed in the denominator of (1) increases about the same amount between 1-200 atm. The result is that $\rho a_c/\omega^2$ is essentially constant in this pressure range.

The thermodynamic quantities c, γ, and C_p are known very accurately. The thermal conductivity or viscosity may therefore be determined when independent measurements of either transport property are available. On the other hand, the measured sound absorption may be used to test the validity theoretical predictions of η and γ with no other measurements involved.

2.4 BULK VISCOSITY

An additional transport property, the translational (or intrinsic) bulk viscosity becomes important at densities approaching the critical density ρ_c. This bulk viscosity should not be confused with that arising from the presence of internal modes which is also present in polyatomic molecules. The translational bulk viscosity may be considered physically due to the fact that correlations between the position of molecules die away in periods longer than the binary collision time. There is therefore a component of pressure which is proportional to the time rate of volume change and which lags behind the pressure associated with binary collisions.

The translational bulk viscosity in liquids has been the subject of controversy. However, recently the experiment (Refs. 15, 16, 17) and theory (Ref. 18) have been shown to be essentially in agreement. In particular, recent studies of argon (Ref. 16) in the dense gaseous region have shown that the ρ^2 variation of bulk viscosity predicted the Rice-Alanatt theory is correct with the experimental error -10%. Following the suggestion of Madigosky the bulk viscosity may be estimated by the Enskog expression

$$\eta' = \frac{4}{9}\left(\frac{\sigma^4}{m^2}\right)\left(\pi\, m K T\right)^{1/2} \chi\, \rho^2 \tag{11}$$

where the Enskog factor χ is taken from Rosenbaum et al. (Ref. 19).

The bulk viscosity enters the sound absorption through the conservation of momentum Eq. (2). The classical absorption is modified by replacing $4/3\,\eta$ in Eq. (1) by $4/3\,\eta + \eta'$. The important comparison for the present discussion is between the excess viscosity

$$\frac{4}{3}\,\eta_e = \frac{4}{3}\,(\eta - \eta_o) \tag{12}$$

and the bulk viscosity. These two quantities are plotted versus pressure at 300°K and 234.6°K in Figure 2 for argon. For temperatures of 300°K and above the Enskog approximation should be slightly higher (< 15%) than the true value of the bulk viscosity. The bulk viscosity is less than 37% of the excess shear viscosity up to pressures of about 100 atm. The bulk

viscosity term is only 15% of the excess thermal conductivity term. Therefore, other measurements of viscosity and theoretical estimates of the bulk viscosity may be used to obtain the excess thermal conductivity from sound absorption measurements up to about 200 atm with a maximum uncertainty of 2%. A better approach is to predict the excess viscosity, thermal conductivity and bulk viscosity theoretically and use the ultrasonic absorption data to test the validity of the theory. Because of the bulk viscosity, the ultrasonic absorption is more sensitive to density effects than other transport property measurements.

2.5 MIXTURES

The sound loss in a mixture includes the usual absorption due to the thermal conductivity and viscosity of the mixture plus terms which arise from diffusion. Diffusive separation of species due to the temperature and pressure gradients in the sound wave leads to an additional term in the energy equation. The theory for low density (~1 atm) gases follows vigorously from kinetic theory (Refs. 20, 21). High density gases should be treated by the techniques of irreversible thermodynamics (Ref. 22). Neglecting the first and second derivatives of compressibility with respect to mole fraction the diffusion losses are given by the low density formula (ρc^2 replacing p)

$$\rho \alpha_D = \frac{2\pi^2 f^2 x_1 x_2 \gamma}{c^3} \left(\beta' + \frac{\gamma - 1}{\gamma} \alpha_T\right)\left(\beta + \frac{\gamma - 1}{\gamma} \alpha_T\right) \rho_o D_{12} \qquad (13)$$

where x is the mole fraction, M the atomic weight, D_{12} the binary diffusion coefficient and α_T the thermal diffusion ratio. The subscripts 1 and 2 refer to the two species ($M_2 < M_1$). The quantities β and β' are given by

$$\beta = \frac{M_2 - M_1}{M} \qquad (14)$$

$$\beta' = \frac{1}{M} \frac{\gamma - 1}{\gamma} \left(\frac{\gamma_1}{\gamma_1 - 1} M_2 - \frac{\gamma_2}{\gamma_2 - 1} M_1\right) \qquad (14a)$$

The γ, γ_1, and γ_2 are the specific heat ratios of the mixture and the pure gases respectively.

The term involving the thermal diffusion factor is relatively small compared to β and β' in cases where the diffusion losses are significant. Diffusion losses for several gas mixtures are given in Table 1. Mixtures of hydrogen and helium with other gases generally show about 50% of the absorption due to diffusion. Sound absorption in these gases may be used to determine diffusion coefficients. In gases such as air and argon-nitrogen mixtures the sound absorption due to diffusion is about 2% of the total absorption. The sum of thermal conductivity and viscosity may therefore be determined as outlined above for pure gases. The 2% losses may be corrected using theoretical diffusion coefficients to give the sum of viscosity and thermal conductivity with better than 0.1% accuracy.

The density behavior of the transport properties of mixtures are not known very well. The thermal diffusion term may be calculated from the best theoretical estimate since its contribution is small. The major factor is the density dependence of the binary diffusion coefficient. Binary diffusion coefficient measurements at high densities suggest that ρD_{12} is more sensitive to density than self-diffusion coefficients and decreases as density increases as indicated by theory (Refs. 25, 26, 27, 28) and experiment (Ref. 24).

Table 1. Contribution of various loss mechanisms to sound absorption in gas mixtures at 1 atm with 1 MHz sound waves (estimates)

Mixture	Temp. °K	$(\alpha p/f^2)_\lambda$ x 10^{-6}	$(\alpha p/f^2)_\eta$ x 10^{-6}	$(\alpha p/f^2)_{\eta'}$ x 10^{-6}	$(\alpha p/f^2)_D$ x 10^{-6}	β	β'	$\frac{\gamma-1}{\gamma}\alpha_T$
He-Ar	300	0.117	0.084		0.175	-1.636	-1.636	0.153
	1000	0.134	0.109		0.228	-1.636		
He-N_2	350	0.0558	0.070	0.029	0.067	-1.500	-1.167	0.143
Ar-N_2	300	0.056	0.106	0.042	0.009	-0.351	-0.685	0.024
	1000	0.161	0.144	0.138	0.012	-0.351	-0.797	0.049
H_2-Ar	300	0.0873	0.087		0.333	-1.808	-2.141	0.096
	1000	0.347	0.149		0.412	-1.808	-2.178	0.121
N_2-O_2	350	0.093	0.105	0.093	0.001	-0.133	-0.133	0.087
	1000	0.151	0.112	0.240	0.000	-0.133	-0.068	0.027
N_2-CO_2	300	0.367	0.105	0.183	0.002	-0.444	-0.217	0.017
	1000	0.688	0.166	0.760	0.000	-0.444	-0.052	0.030

The absorption due to the diffusion coefficient, therefore, decreases with increasing pressure. An examination of Eq. (13) and the sound speed versus pressure curves shows that ρa_D decreases about 30% in 100 atm due to the c^3 in the denominator. There may be an additional decrease of about 10% due to the decrease in the diffusion coefficient in the same pressure range.

2.6 INTERNAL MODES-ROTATIONAL RELAXATION

The absorption due to thermal relaxation at high densities may be derived by breaking the internal energy U into a translational part and a component due to internal modes. Coupling a relaxation equation (Refs. 10, 15) to the conservation equations then leads to the correct expression for sound absorption due to internal modes. However, it is more rigorous at high densities to use arguments based on irreversible thermodynamics. The resulting expressions are identical to the usual low density expressions.

The only question remaining is the effect of density on the relaxation time. The main event leading to a change of the internal state of a molecule is a hard binary collision. The number of such collisions per second should be directly proportional to the density. The product of relaxation time and the density, $\rho\tau$, will be a constant at all densities if the probability (transition probability) that a collision will result in a change of internal state is constant. This assumption is plausible from a physical point of view. This assumption is reasonable because the colliding molecules are perturbed by a hard collision much more than by the long range interaction with their neighbors up to high densities. Measurements of vibrational relaxation times (Refs. 14, 29) show that $\rho\tau$ is constant at densities up to about twice the critical density. The same result holds up to at least 100 psi for rotational relaxation in N_2 as indicated by the agreement between theory and experiment in Figure 9. The absorption due to rotational relaxation at high densities reduces to

$$\rho a_{rot} = \frac{\pi}{8} \frac{\omega^2}{c} \frac{\gamma - 1}{C_p} C_i \left(\frac{\eta_o}{RT}\right) Z_{rot} \qquad (15)$$

where η_o is the low density viscosity and R is the gas constant per gram. The low density viscosity enters because the binary collision relaxation (τ_c) time was calculated assuming $\rho\tau_c$ was a constant, that is

$$\tau_c = \frac{\rho_o}{\rho} \tau_{co} = \frac{\pi}{4} \frac{\rho_o}{\rho} \frac{\eta_o}{p_o} \tag{16}$$

The subscript o refers to the low density limit. The density sound absorption product indicated by Eq. (15) is essentially constant between 1-100 atm.

2.7 SUMMARY

The above discussion shows how, in principle, the transport properties of gases may be determined at high pressures using ultrasonics. The sum of thermal conductivity and viscosity may be determined from Eq. (10). The absorption due to relaxation of internal modes may be subtracted from the total absorption to obtain the sum of thermal conductivity and viscosity in diatomic and triatomic gases. The frequency may be chosen sufficiently high so that all internal modes except rotation contribute less than 0.1%. Equation (15) then is typically 30% correction term. Finally, ultrasonic absorption in mixtures may be used to measure diffusion coefficients or the sum of viscosity and thermal conductivity depending on the difference in molecular weights of the species involved. Diffusion losses in mixtures of helium and hydrogen with heavier gases are ~50% of the total. Therefore, absorption and diffusion coefficients of such mixtures may be obtained. On the other hand, diffusion losses in mixtures of other gases are small (typically less than ~1%) and the sum of viscosity and thermal conductivity may be determined as described above.

SECTION III

APPLICATION OF THE ULTRASONIC TECHNIQUE TO HIGH PRESSURE GASES

3.1 PULSE ECHO THROUGH TRANSMISSION TECHNIQUE

High pressure cells suitable for measuring ultrasonic absorption and dispersion have used both movable probes (Ref. 30) and fixed probes (Ref. 31). Movable probe apparatus yields curves of amplitude versus position and transit time versus distance directly. The fixed probe technique must use echoes to obtain more than one path length. In addition, corrections for the diffraction losses and transmissivity of the ultrasonic mirrors must be made. The advantages of the fixed probe technique are due to its mechanical simplicity. There are no errors associated with variation of alignment with position. There are no rotating shafts to seal against high pressure. Finally, the mechanical simplicity of the fixed path technique is very important at high temperatures (500°C) and pressures (8000 psi).

The fixed path probes used in the present experiment are shown in Figure 3. The details of the pressure cell are not shown. The probes are, however, attached to the cover and the floor of a steel pressure bomb with suitable high pressure inlets for gas, electricity, internal water cooling, thermocouples, and coaxial lines for the rf pulses which drive the ultrasonic probes. The pressure cell used with the probes is internally cooled so that temperatures up to ~2000°K at pressure up to 200 atm could be used. This cell (referred to as I) was used to obtain the sound absorption measurements reported below. A second cell (referred to as II) externally heated (built by Aminco) which will go to 1000 atm at 300°K and 400 atm at 800°K was used to obtain the sound speed reported between 100 atm and 400 atm. The probes in cell II were similar to those shown in Figure 3 except that both probes were mounted on the cover of the pressure cell.

The major problems associated with acoustic measurements in gases at high temperature and pressure are alignment, acoustic isolation, rf transmission, ringing and diffraction corrections. The probes are held in alignment by the stainless steel tubing which also serves as the ground for the rf transmission lines. Ceramic insulators allow the coaxial line to be used at high temperatures. The probes are roughly aligned by maintaining the mechanical parts as true as possible. However, final alignment must be adjusted while examining the first pulse and the echo by an oscilloscope. The previous systems mentioned above used a solid tube for alignment.

The sound energy is more easily transmitted through the transducer mount into the walls of the pressure cell than through the desired gas path. This is because of the large mismatch between the gases and the solids in the low pressure range (ρ < 100 atm). Improper acoustic isolation leads to sound transmission through the walls which overshadows the desired signal through the gas. The only technique which provides sufficient isolation between the cell walls and the transducer under the conditions of the present experiment is minimum mechanical contact between the receiver and the transmitter. Mounting the probe holder on the coaxial line as shown in Figure 3 provides minimum mechanical contact.

The remaining features of probe design are best understood in terms of the through transmission multiple echo technique employed in the present experiments. The photographs in Figure 4 show a series of ultrasonic pulses. The first pulse in each photograph is the transmitted pulse as it encounters the receive transducer. The following pulses arise by multiple reflections in the gas cavity between the transmitter probe and the receive probe. Thus, the distance between the first pulse and the first echo is twice the probe separations. There is a "tail" on each pulse which interferes with the following pulse at close separations. The tail, referred to as ringing, is due to acoustic energy trapped in the transducers. The ringing may be damped for a crystal radiating into air by backing the transducer with a lossy material. The damping material used in the present experiment was a short circuited PZT-5 ceramic transducer.

The attenuation of the ultrasonic wave is given by the natural logarithm of amplitude ratio of the first pulse and the first echo, divided by the path length. The measured attenuation is due to absorption during reflection, diffraction losses and absorption due to transport and relaxation phenomena. The attenuation coefficient due to transmission at reflecting surfaces may be neglected at pressures up to 100 atm because the gas acoustic impedance is small compared to the solid. The effective attenuation coefficient due to reflection losses is:

$$\alpha_{ref} = -\frac{1}{2d} \ln \left(\frac{\rho_g c_g}{\rho_s c_s} \right) \tag{17}$$

where $\rho_g c_s$ are the products of the sound speed and the density of the gas and the solid, respectively. The absorption coefficient due to reflection losses in the present experiment which ranges between 5×10^{-5} to 5×10^{-3} nepers/cm is negligible.

The diffraction losses depend only on the wavelength of the ultrasonic wave, the diameter of the radiator and the path length. The simplest loss of this type is due to beam spreading. That is, the energy diverges so that a certain fraction of the transmitted beam does not intercept the receiver. Beam spreading losses amount to about 0.01 nepers/cm under the worst conditions of the present experiment.

The term "diffraction losses" (Ref. 32) is more commonly used to describe apparent losses due to deviations from constant pressure across the beam which are inherent in the piston radiator field. In the MHz frequency range for typical radiator dimensions (a ~1 cm) diffraction losses are small compared to the absorption due to transport phenomena. However, due to the mounting of the transducer in a slight depression, diffraction losses are much larger than usual. Typically, α_{diff} is about 0.2 nep/cm in the present experiments. A flush mounted transducer has lower diffraction losses but is more difficult to electrically ground.

3.2 DATA REDUCTION

The separation of the attenuation due to diffraction from the absorption due to transport and relaxation effects may be accomplished many ways. The difference between the measured low pressure (~1 atm) attenuation in the pressure cell and the theoretical absorption could be used to obtain the diffraction losses. The method adopted in the present experiment takes advantage of the pressure dependence of the various loss mechanisms. As mentioned in the theory section, the classical absorption varies as $1/\rho$. The absorption due to diffraction losses and reflection losses is essentially independent of density. Therefore, a plot of attenuation versus $1/\rho$ should be a straight line

$$\alpha = \frac{A}{\rho} + B \tag{18}$$

The constant B is the diffraction loss. A check on the validity of this procedure is provided by the fact that A should be equal to the density times the classical absorption at atmospheric pressure. The linear relation clearly holds as may be seen from Figure 5. In addition, the coefficient of the $1/\rho$ term is equal to the classical absorption calculated from measured values of viscosity and thermal conductivity.

It should be noted that this technique applies over a limited pressure range. The assumptions are that reflection losses (α_r) and the sound speed (or wavelength) do not change much over the pressure range of the data.

3.3 SUM OF THERMAL CONDUCTIVITY AND VISCOSITY MEASUREMENTS IN THE ARGON-NITROGEN SYSTEMS

Measurements of sound absorption and velocity in argon, nitrogen and argon-nitrogen mixtures at pressures up to 100 atm illustrate the type of information which has been obtained. The ρa_c versus pressure is shown in Figure 6 for argon. The specific heat ratio and sound speed from the present measurements were used with independent thermal conductivity and viscosity and C_p measurements to calculate ρa_c. The agreement between the various experiments is excellent over the whole pressure range. The pressure effect on viscosity and thermal conductivity over the pressure range of 100 atm amounts to about 25%. The bulk viscosity contributes about 10% of the excess or 2% of the total absorption in the gases measured.

The normalized absorption (ρa) measured in nitrogen is shown in Figure 7. Nitrogen has the additional feature of rotational relaxation. The classical absorption is shown by the solid line in Figure 7. The absorption due to rotational relaxation was calculated using a rotational collision number $Z_{rot} = 4.25$, determined from ultrasonic measurements at atmospheric pressure. The total absorption passes through the center of the data over the entire pressure range.

The sound absorption versus pressure in the argon-nitrogen mixtures was difficult to handle because of the uncertainties associated with the properties of mixtures at high pressures. The transport properties of mixtures may have a different pressure behavior than pure gases because of the pressure dependence of the diffusion coefficients. However, the technique of fitting the normalized absorption to a linear function of pressure was applied. The procedure is justified by the fact that the coefficient of $1/\rho$ does come out to be equal to the known absorption at atmospheric pressure. The rotational collision number was determined for the mixture from atmospheric pressure measurements and Eq. (15). The sum of viscosity and thermal conductivity in terms of ρa_c was added to the rotational contribution to compare with the measured ρa. The results are displayed in Figures 8 and 9 along with the theoretical total absorption. It should be pointed out that the sum of viscosity and thermal conductivity would be obtained by subtracting the rotational losses from the total absorption. Accurate specific heat data, γ and C_p, necessary to reduce ρa_c to transport properties are not available. This shortcoming will be removed by measurements of sound speed versus pressure at several temperatures above 300°K.

3.4 SUM OF THERMAL CONDUCTIVITY AND VISCOSITY MEASUREMENTS IN THE HELIUM-ARGON SYSTEMS

Absorption versus pressure in a 0.5 helium-0.5 argon mixture is shown in Figure 10. These measurements were suggested by J. Sengers for comparison with some high density results on diffusion coefficients in a Lorentz gas (Refs. 26, 27, 28). The absorption due to diffusion is about one-half of the total absorption. The classical absorption shown in Figure 10 was constructed by extrapolating $\rho \alpha_c$ from low pressure values. The contribution of diffusion was calculated by extrapolating one atmosphere diffusion coefficients theoretically (Ref. 28) to high pressures. There are some indications (Ref. 33) that the thermal diffusion factor could increase by a factor of 3 at high pressures. This effect was included in the calculation of diffusion losses. The total absorption coefficient thus calculated agrees remarkably well with the measured values.

The agreement between theory and experiment in Figure 10 shows that the theory is fundamentally sound. However, the usefulness of the ultrasonic technique for the determination of diffusion coefficients at high pressures is limited by several factors. First, the above calculations show that the size of the diffusion losses decreases rapidly as pressure increases due to the c^3 in the denominator of Eq. (13). Second, the thermal diffusion coefficient becomes more important at high pressures. For He-CO_2 mixtures the $\frac{\gamma - 1}{\gamma} \alpha_T$ factor increases to about 60% of the diffusion term in Eq. (13) at 100 atm.

3.5 SPECIFIC HEAT RATIO DETERMINATIONS FROM SOUND SPEED MEASUREMENTS

Sound speed measurements were obtained simultaneously with the absorption measurements. The temperature was measured with two thermocouples (see Figure 8). The sound speed in this case may be used to determine the thermodynamic properties of the gas. Specific heat ratios were obtained from compressibility measurements (Ref. 34) and the sound speeds for argon and nitrogen. Specific heat ratios for the argon-nitrogen mixtures were derived based on the assumption that the excess viral coefficients were small (Ref. 35). Specific heat ratios were not determined for the helium-argon mixtures because the excess viral coefficients may be large (Ref. 35).

The major part of the pressure dependence of the sound speed comes from the specific heat ratio. The factor

$$\frac{z}{1 - \frac{p}{z}\left(\frac{\partial z}{\partial p}\right)_T} \tag{19}$$

in Eq. (9) differs from 1.00 at most by 2% in the 1-100 atm range for the argon-nitrogen system. Thus very accurate specific heat ratios may be obtained from rough compressibility measurements and accurate sound speed measurements.

A schematic diagram of the electronics used for the sound speed measurements is shown in Figure 11. The first pulse and the first echo are superimposed on a dual beam oscilloscope using delayed triggers. The delayed scope trigger is obtained by putting the transmitter trigger through a two-channel digital delay generator. The oscilloscope traces are delayed to cancel the transit time of the respective pulses to within 0.1 μsec. Since the transit times are typically 150 μsec this procedure gives a precision of better than 0.1%. Delays inherent in the triggers and errors in the ultrasonic path length were corrected with calibration in argon and helium at 1 atm. A typical oscilloscope trace is shown in Figure 12.

The sound speed versus pressure curves for the argon-nitrogen system is shown in Figure 13. Where data were available the present data are in agreement with other work to within 0.5%. The temperature, pressure and sound speed are tabulated in Tables 2 and 3. Also shown are values of specific heat ratio γ derived from the sound speed and compressibility measurements using Eq. (9). The mixtures again were a problem because compressibilities were not available. Further measurements at different temperatures are in progress to obtain thermodynamic properties from the sound speed measurements alone.

3.6 SUMMARY

A cell for measuring sound absorption and sound speed at pressures up to 1000 atm and temperatures up to 800°K has been built and tested. Attenuation measurements have been made in this apparatus with better than 1% precision. There are large diffraction losses (~0.2 nep/cm) inherent to the acoustic probes used due to the recessed mounting of the acoustic transducer. Since the diffraction losses had to be subtracted from the total attenuation coefficient, the precision of the absorption measurements reported was reduced as much as 15% at the highest pressures. While these experiments were in progress a new flush mounting technique was developed reducing the diffraction losses by a factor of 10 (to 0.02 nep/cm). This increase in precision will be reflected in future absorption measurements.

Measurements of absorption in the argon-nitrogen system show that the experiment and theory are in agreement. Thermal conductivities could be obtained from the smoothed sound absorption data and other viscosity measurements. However, more accurate measurements are in progress. The measurements of sound absorption in the helium-argon mixture show that diffusion coefficients are difficult to obtain from absorption measurements at high pressures. This is due to the decrease of the diffusion losses with an increase in pressure. On the other hand, the decrease of significant diffusion losses means that accurate measurements of thermal conductivity and viscosity may be obtained from absorption measurements in gas mixtures at high pressures.

Finally, sound speed versus pressure measurements were made in the argon-nitrogen and argon-helium systems. The major reason for sound speed variation with pressure below 100 atm is the change in the specific heat ratio; therefore, specific heat ratios were derived from the sound speed measurements in the argon-nitrogen system. Because the unknown excess viral coefficients are large in the helium-argon mixtures no attempt was made to obtain specific heat ratios for these gases. Variation of pressure above 100 atm and variation of temperature will provide both compressibility and specific heat ratio from sound speed alone. Thermodynamic properties of gas mixtures at pressures above 200 atm are not well-known; therefore, the sound speed measurement is very useful.

Table 2. Sound speed data in the argon-nitrogen systems

Nitrogen

0-200 psi Cell I

Pressure p atm	Temp. T °K	Sound Speed C m/sec	γ
3.93	300.3	353.0	1.401
3.93	299.8	353.2	1.405
14.67	299.6	355.2	1.422
21.54	299.6	356.3	1.428
28.35	299.8	358.3	1.448
34.88	299.4	359.7	1.455
41.61	299.0	360.3	1.463
55.22	298.4	362.9	1.484
62.36	298.6	365.2	1.504
68.62	298.6	367.3	1.509
82.90	299.0	372.5	1.534
88.76	297.8	374.6	1.550
88.62	297.8	372.2	1.531
95.69	297.8	375.9	1.553
102.36	297.8	378.4	1.565
102.22	297.8	378.4	1.565

0-30,000 psi Cell II

Pressure p atm	Temp. T °K	Sound Speed C m/sec	γ
8.84	302.6	349.2	1.361
20.41	302.5	357.6	1.425
40.82	302.6	360.9	1.449
61.22	302.7	366.4	1.493
81.29	303.3	371.6	1.505
102.04	303.5	378.1	1.533
122.44	303.5	383.9	1.556
142.86	303.2	395.4	
163.37	302.7	407.6	
184.0	302.3	411.9	
225.5	301.3	445.9	
264.3	301.9	464.2	
295.2	301.3	488.0	
328.6	301.3	505.7	
357.8	301.2	527.0	

50 N_2-50 Ar

p	T	C	γ
7.75	295.6	327.1	
14.69	296.5	328.6	
21.43	299.2	330.2	
28.23	297.7	331.7	
35.44	297.7	333.1	
41.70	297.8	334.4	
49.18	297.7	334.9	
55.24	297.7	339.2	
61.43	297.7	338.7	
68.37	297.7	339.2	
74.97	297.7	342.0	
80.00	298.2	343.0	

p	T	C	γ
68.03	306.1	339.9	
81.63	305.9	342.6	
95.24	306.0	349.9	
109.5	305.6	355.5	
122.8	305.0	360.0	

Table 2. Sound speed data in the argon-nitrogen systems (cont' d)

Argon

0-200 psi Cell I

Pressure p atm	Temp. T °K	Sound Speed C m/sec	γ
7.35	299.8	320.6	1.648
21.91	297.6	322.0	1.686
28.30	297.7	322.9	1.708
34.22	297.7	323.8	1.720
42.25	297.7	324.8	1.779
48.64	297.7	326.9	1.811
54.83	297.7	326.6	1.808
61.84	298.0	328.1	1.844
68.10	298.0	329.5	1.849
74.70	297.8	330.2	1.863
81.78	298.2	332.2	1.890
88.44	298.2	333.9	1.915
95.24	298.2	335.6	1.940
102.04	298.3	337.4	1.968

0-30,000 psi Cell II

Pressure p atm	Temp. T °K	Sound Speed C m/sec	γ
60.88	304.9	328.2	1.787
81.29	304.8	331.4	1.840
101.4	304.4	340.2	1.961
121.8	304.4	343.6	2.018
140.5	303.2	350.5	
163.3	303.2	356.5	
181.6	303.2	368.1	
204.8	303.9	377.2	
224.8	303.9	384.5	
245.9	304.2	400.4	
266.3	304.6	407.3	
289.1	305.6	418.8	
311.6	305.4	433.3	
329.9	305.4	443.4	
345.6	304.4	453.5	

0.9 Ar-0.1 N_2

p	T	C	γ
7.96	300.4	323.8	
14.35	301.0	323.8	
31.64	301.0	325.0	
28.57	301.0	326.1	
35.24	301.0	327.6	
42.38	301.0	328.5	
48.98	301.0	329.0	
55.24	301.0	330.4	
61.50	301.0	331.2	
68.64	301.0	332.1	
75.10	301.2	334.1	
81.50	301.0	334.8	
82.30	301.0	336.6	
95.10	301.2	338.4	
101.91	301.2	340.4	

Table 3. Sound speed data in a 0.474 argon-0.526 helium mixture

0-200 psi Cell I				0-30,000 psi Cell II			
Pressure	Temp.	Sound Speed		Pressure	Temp.	Sound Speed	
p atm	T °K	C m/sec	γ	p atm	T °K	C m/sec	γ
7.35	299.0	426.4					
14.69	299.0	428.4					
21.77	299.0	430.4					
28.16	296.8	430.6					
35.10	297.4	432.1					
41.77	297.4	434.8					
41.77	296.4	432.5					
48.44	297.4	436.1					
49.52	296.6	436.7					
54.97	297.7	430.8					
61.77	297.7	441.0					
68.98	297.7	443.1					
75.10	297.9	445.3					
81.90	297.9	447.1					
89.12	297.9	447.5					
96.26	297.9	449.3					
102.04	297.9	451.1					

SECTION IV
SCHLIEREN INTERFEROMETER

4.1 WOLLASTON PRISM DIFFERENTIAL INTERFEROMETER

A differential interferometer measures the index of refraction gradient. This in turn is directly proportional to the density gradient for many systems of interest. The measurement of thermal conductivity by conventional techniques requires temperature derivatives to be calculated from temperature measurements. Since the differential interferometer measures gradients directly in the gas it has some interesting applications for thermal conductivity measurements. The problem is to find flows where the temperature gradients in the conservation of energy equation may be eliminated in favor of the density gradient. The temperature field about a body in free convection and the end wall boundary layer are two such applications.

The "schlieren" or Wollaston prism differential interferometer is a very useful device in its own right. It is simple and not as sensitive to vibration as the usual interferometer. Wollaston prism differential interferometers have been described by Lamb and Schreiber (Ref. 6) for arc applications and by Oertel (Ref. 36) for shock tunnel applications. The primary interest in this instrument is based on Smeets (Refs. 37, 7) thermal conductivity determinations using the end wall boundary layer.

A schematic of the basic apparatus is shown in Figure 14. The light from any point in the FX12 mercury light source is polarized so the electric vector is 45° to the optical axis of the Wollaston prism. The prism is constructed of two optically active quartz wedges (Ref. 6) cemented together with crossed optical axis. The Wollaston prism breaks the polarized light into two rays of equal intensity diverging at an angle ϵ. The lens L_1 is focused through the Wollaston prism and the polarizer into the center of the light source. Therefore the diverging rays from the prism are converted into parallel rays by L_1. In addition, the rays are separated by a distance d. A similar system recombines the two rays on the film plane of the camera. The lens L_2 is focused on an imaginary object in the center of the test region.

When the test region is uniform a fringe pattern develops due to phase shifts within the two Wollaston prisms (Ref. 6). The location of the fringes (or equivalently the phase shifts in the system) depends on the wavelength of the light. Thus red fringes do not form at the same place on the photographic plane as the yellow or blue fringes. Visually

the interference pattern from white light separates the colors. On a photograph the effect is to show fuzzy fringes since the camera does not discriminate among the colors. An example of this effect is shown in Figure 15 where photographs of the fringe field with a 500Å wide filter and a 100Å wide filter are displayed. Very good fringes are obtained using a 100Å wide filter centered on the 4671Å xenon line.

4.2 THERMAL GRADIENTS ABOUT A HORIZONTAL CYLINDER IN FREE CONVECTION

The fringe field for a long ceramic cylinder held at approximately 900°C in air with free convection is shown in Figure 16. The horizontal gradients are obtained aligning the interferometer so that the fringes are vertical. Similarly realigning the interferometer the vertical gradients may be obtained as shown in the upper photograph. The vertical fringe along the stagnation line shows that the horizontal gradient is zero. The vertical gradients are a maximum along the same line. The thermal conductivity could be determined by a similar experiment if the convective flow velocity could be determined. This experiment would avoid many of the radiative and convective corrections which become important at high temperatures and pressures in conventional thermal conductivity measurements.

4.3 THEORY OF THERMAL CONDUCTIVITY MEASUREMENTS IN THE END WALL BOUNDARY LAYER

The detailed theory of the Wollaston prism differential interferometer is given in References 6 and 26. The basic theory for the thermal conductivity measurement in the end wall boundary layer may be understood by considering the two rays created by the Wollaston prism as they pass through the shock tube. The ray traveling through the cooler gas travels at a slightly slower speed because the density of the gas increases as it cools. The two rays therefore develop a phase difference in the test gas given by

$$\frac{\Delta\phi}{2\pi} = \frac{\ell}{\lambda} \left(n_{+d} - n_{-d}\right) \tag{20}$$

where ℓ is the length of the test section, λ the wavelength of the light, n_{+d} and n_{-d} are the indexes of refraction a distance $y \pm \frac{d}{2}$ from the end wall. The theory of the optics gives the fringe shift Δs in terms

of the phase shift and the undisturbed fringe separation s by the relation

$$\Delta s = \frac{\Delta\phi}{2\pi} s = s \frac{\ell}{\lambda} (n_{+d} - n_{-d}) \tag{21}$$

or finally multiplying and dividing by the ray separation, d, we obtain a relation between the density (or index of refraction) gradient and the fringe shift

$$\frac{d\rho}{dy} = \frac{1}{a} \frac{dn}{dy} = \frac{1}{a} \frac{\Delta s}{s} \frac{\lambda}{\ell} \frac{1}{d} \tag{22}$$

where a is the Gladstone-Dale constant for the gas in question, ρ the density of the gas and y the distance from the end wall.

Equation (22) relates the measured fringe shift Δs to the density gradient. The relations needed to obtain thermal conductivity come from the boundary layer equations. A suitable way of writing the energy equation was derived in last year' s final report (Ref. 7). The equation is

$$\ln \frac{\left(\frac{\partial\rho}{\partial y}\right)_1}{\left(\frac{\partial\rho}{\partial y}\right)} = \frac{1}{4t} \frac{C_{pe}\rho_e}{\lambda_e} (y-y_1)^2 + \frac{\eta_e}{\sqrt{2t}} \frac{C_{pe}}{\lambda_e} (y-y_1) + C \tag{23}$$

where the subscript 1 refers to the reference point close to the end wall, C_{pe} is the specific heat, and λ_e the thermal conductivity. The similarity parameter η_1 is defined by

$$\eta_1 = \frac{1}{\sqrt{2t}} \int_0^{y_1} \rho \, dy \tag{24}$$

and t is the time measured from the time that the shock wave is reflected from the end wall.

4.4 APPLICATION OF DIFFERENTIAL INTERFEROMETER TO THE WALL BOUNDARY LAYER

The steps involved in applying Equations (22) and (23) to the measurement of thermal conductivity are (1) derive the density gradient from the measured fringe shift on the interferogram of the end wall boundary layer; (2) fit the density gradient to the quadratic function of distance from the reference point $(y_1-y)^2$. The thermal conductivity is given by the coefficient of the quadratic term in Eq. (23). Additionally, the similarity parameter η_1 may be estimated to within a few percent and the linear term in (23) may then be used to determine thermal conductivity.

There are several important points about Eq. (23) which minimize experimental errors in the thermal conductivity measurements. First, since the ratio of the density gradients at two points is the important property in Eq. (23), the proportionality factors in Eq. (22) do not need to be known, that is,

$$\frac{\left(\frac{d\rho}{dy}\right)_1}{\left(\frac{d\rho}{dy}\right)} = \frac{\Delta s_1}{\Delta s} \tag{25}$$

In addition, the magnification in the direction parallel to the end wall drops out. The location of the end wall is also not necessary because only the differences in distance from the wall occur in the final expression for thermal conductivity (Eq. 23). The magnification in this direction is important and is easily determined by inserting an accurately known cylinder in the test section and photographing it. Finally, the accuracy of the linearization which leads to Eq. (23) is automatically determined by the size of the constant (C) which approaches zero as the deviation from free stream conditions decreases over the portion of the boundary layer in the schlieren field.

Some measurements of the fringe displacement on a typical end wall schlieren interferogram are shown in Figure 17. The position of the end wall is indicated by the vertical arrow. The data are measured points on the fringe. Taking the factor of two magnification on the photograph into account the fringes are discernable to within 0.1 mm

of the end wall. The separation of ordinary and extraordinary rays in the test section (the rays which interfere to give the fringes) is about 0.047 mm, much smaller than the boundary layer. The total boundary layer is 3 mm thick. The fringes are straight lines with ~20% slope in the uniform part of the reflected shock region. Closer to the end wall in the boundary layer the fringes bend upward. The total temperature change in the part of the boundary layer affecting the fringes is about 3000°K. This means that half of the temperature drop is in the outer 3 mm of boundary layer and half of the drop is in the remaining 0.1 mm. The temperature gradient near the end wall is very steep, while the outer regions show small temperature gradients. This is the basis of the linearization of the energy equation to give the useful relation Eq. (23).

SECTION V

THERMAL CONDUCTIVITY MEASUREMENTS WITH SCHLIEREN INTERFEROMETER

The thermal conductivity of nitrogen, 0.25 argon-0.75 helium mixture, and air, was measured at temperatures up to 5000°K and pressures up to 6 atm using the schlieren interferometer on the end wall of the shock tube. The free stream temperature and pressure of the test gas behind the reflected shock were determined from incident shock speed measurements (Ref. 38). The transit time determined from heat transfer gauges 106.05 cm and 14.61 cm from the end wall was used to determine the wave speed. In addition, an end wall heat transfer gauge was used.

A heat transfer trace is shown in Figure 17 along with a schlieren interferometer photograph of the end wall boundary layer. The upper heat transfer trace is the side wall gauge response, the lower trace is the end wall gauge response. The break in the end wall gauge response indicates the end of the uniform conditions in the gas close to the end wall. A burst of rf from the flash tube interrupting uniform end wall trace indicates when the schlieren photograph was taken. The time between the arrival of the shock wave at the end wall (the step in the end wall trace) and the time of the schlieren photograph is given by the position of this rf pickup. This is the time which should be used in Eq. (23).

Some measurements of fringe displacements versus distance from the end wall for a measurement in air are shown in Figure 18. The ratio of $\frac{\Delta s}{s}$ is averaged over a number of fringes. The resulting $\frac{\Delta s}{s}$ data are fit to a quadratic function of distance as described above in the discussion of Eq. (23). The resulting thermal conductivity values are tabulated in Table 4.

Table 4. Thermal conductivity of gases measured by the schlieren technique

Temperature °K	Pressure atm	Thermal Conductivity mw/cm °K
	Nitrogen	
2620	2.29	2.10
4373	4.86	3.20
4707	5.44	3.41
5141	6.34	4.10
	Air	
2246	1.87	1.87
2258	2.04	2.26
2398	2.08	2.15
2550	1.15	2.30
2572	0.29	2.25
2999	0.30	3.00
3157	0.57	2.88
4539	5.53	3.10
	0.75 He-0.25 Ar	
5571	1.24	5.43

SECTION VI
SUMMARY

Sound absorption and sound speed measurements were shown to be a useful technique for measuring gas thermodynamic and transport properties at high pressure. The sum of viscosity and thermal conductivity can be determined from sound absorption measurements in a wide variety of pure gases and gas mixtures. Measurements of sound absorption in argon-nitrogen and argon-helium mixtures were made at 300°K and pressures up to 100 atm. Good agreement between theory and experiment was obtained. These measurements demonstrated that losses due to relaxation and diffusion are adequately described by well-known theory. Therefore, relaxation and diffusion losses may be determined and subtracted from the total absorption to obtain the sum of viscosity and thermal conductivity.

The sound absorption is more sensitive to the density dependence of transport properties than other transport property measurements because of the translational (intrinsic bulk viscosity. A theoretical relation between bulk viscosity and viscosity would be useful. Such a relationship can probably be established rigorously in the near future. For this reason ultrasonic absorption provides support for long range theoretical developments in high density gas transport theory.

Thermodynamic properties are also obtained from sound speed measurements. Thermodynamic properties of mixtures at high pressure are not generally available; therefore, this information is valuable in its own right.

Sound speed measurements were made (with accuracies better than 0. 1%) in the argon-nitrogen and argon-helium systems at 300°K at pressures up to 400 atm. Specific heat ratios were deduced for the argon-nitrogen system. Measurements of sound speed at several temperatures and at pressures above 100 atm will allow a complete thermodynamic description of these gases to be obtained.

The schlieren interferometer was analyzed for thermal conductivity measurements at temperatures of 300°K and above. Density gradient profiles were measured in the end wall boundary layer of the shock tube. The theory of end wall boundary layer was used to derive an expression for thermal conductivity in terms of the measured density gradient profiles. Measurements of thermal conductivity of nitrogen and air were made using the schlieren interferometric technique. This technique is, in the authors' opinion, the best way to measure thermal conductivity at temperatures between 3000°K and 8000°K.

REFERENCES

1. Sengers, J. V., Sengers, J. M. H. Levelt, "Critical Phenomena", Chem. Eng. News 46 (1968).

2. Senger, J. V., Michels, A., "The Thermal Conductivity of Carbon Dioxide in the Critical Region", in progress in International Researcher Thermodynamic and Transport Properties, Academic Press, New York (1962) (ASME).

3. Hanley, H. I. M., Childs, G. E., "Discrepancies Between Viscosity Data for Simple Gases", Science 159, 1114 (1968).

4. DiPippo, R., Kestin, Jr., "The Viscosity of Seven Gases Up To 5000°C and Its Statistical Interpretation", in 4th Symposium on Thermophysical Properties, ASME, New York (1968).

5. "Evaluation of High Temperature Gas Transport Properties", AVCO Corp., NASA CR-575 (1966).

6. Schreiber, P. W., Schumaker, K. H., Benedetto, K. R., "Experimental Determination of Plasma Transport Properties", 8th Conference on Thermal Conductivity, Purdue (1968).

7. Carnevale, E. H., Carey, C., Marshall, T and Uva, S., "Experimental Determination of Gas Properties at High Temperatures and/or Pressures", AEDC-TR-68-105 (1968).

8. Uva, S., "Ultrasonic Propagation in High Temperature Gases and Plasmas", Ph. D. Thesis, Boston College (1968).

9. Carnevale, E. H., Larson, G., Lynnworth, L. G., Carey, C., Panaro, M. and Marshall, T., "Experimental Determination of Transport Properties of High Temperature Gases", NASA-CR-789 (1967).

10. Greenspan, M., "Translational Dispersion in Gases", in Proceedings of the International School of Physics, "Enrico Fermi" Course XXVII, Academic Press, New York (1963).

11. Hug, W. F., Evans, D. L., Tankin, R. S., Cambel, A. B., "Measured Index of Refraction of an Argon Plasma", ARL 66-0140 (1966) (Wright-Patterson Air Force Base, Ohio).

REFERENCES (cont' d)

12. Hug, W. F., Evans, D., Tankin, R. S., Cambel, A. B., "Measured Index of Refraction for Argon Plasma", Phys. Rev. 162, 117 (1967).

13. Hug, W. F., Tankin, R. S., Cambel, A. B., "Measurement of the Refractive Index in an Argon Plasma at 6328Å and 1.15μ", ARL 67-0218 (1967) (Wright-Patterson Air Force Base, Ohio).

14. Litovitz, T. A., "Ultrasonic Relaxation in Liquids", in Proceeding of the International School of Physics, "Enrico Fermi", Academic Press, New York (1963).

15. Naugle, D. G., "Excess Ultrasonic Attenuation and Intrinsic Volume Viscosity in Liquid Argon", J. Chem. Phys. 44, 741 (1966).

16. Madigosky, W. M., "Density Dependence of the Bulk Viscosity in Argon", J. Chem. Phys. 46, 4441 (1967).

17. Singer, J. R. and Lunsford, J. H., "Ultrasonic Attenuation and Volume Viscosity in Liquid Nitrogen", J. Chem. Phys. 47, 811 (1967).

18. Gray, P. and Rice, S. A., "On the Kinetic Theory of Dense Fluids XVIII The Bulk Viscosity", J. Chem. Phys. 41, 3689 (1964).

19. Rosenbaum, B. M., Oshen, S. and Thodos, G., "Thermal Conductivity of Argon in the Dense Gaseous and Liquid Regions", J. Chem. Phys. 44, 2831 (1966).

20. Carey, C., Carnevale, E. H. and Uva, S., "Ultrasonic Determination of Diffusion Coefficients in a Helium-Argon Mixture", J. Chem. Phys., to be published (1968).

21. Kohler, M., "Schallabsorption in binären Gasmischunzen", Zeit. Für Physik 127, 41 (1949).

22. Bahtia, A. B., Ultrasonic Absorption, Oxford University Press, London, pp. 377-383 (1967).

23. Bradley, R. S., High Pressure Physics and Chemistry, Vol. I, Academis Press, London, p. 109 (1963).

REFERENCES (cont' d)

24. DePaz, M., "Diffusion Experiments with Simple Gases in the Critical Region", in Proceedings of the Fourth Symposium on Thermophysical Properties (J. R. Moszynski, Editor), ASME New York (1968).

25. Chapman, S. and Cowling, T. G., The Mathematical Theory of Non-Uniform Gases, Cambridge University Press, pp. 292-294 (1960); see also Herschfelder, J. O., Curtis, C. F. and Bird, R. B., Molecular Theory of Gases and Liquids, John Wiley and Sons, New York, p. 646 (1954).

26. Weijland, A. and van Leeuwen, J. M. J., "Non-Analytic Density Behavior of the Diffusion Coefficient of a Lorentz Gas", Physica 38, 35 (1968).

27. van Leeuwen, J. M. J. and Weijland, A., "The Density Expansion of the Diffusion Coefficients of a Lorentz Gas", in Statistical Mechanics Foundations and Applications (T. A. Bak, Editor), Benjamin, New York, p. 335 (1967).

28. van Leeuwen, J. M. J. and Weijland, A., "The Diffusion Coefficient of a Lorentz Gas", Physica 36, 457 (1967).

29. Litovitz, T. A., "Theory of Ultrasonic Thermal Relaxation Times in Liquids", J. Chem. Phys. 26, 469 (1957).

30. Litovitz, T. A. and Carnevale, E. H., "Effect of Pressure on Sound Propagation in Water", J. App. Phys., 26, 816 (1955).

31. Johnson, W. H., Jr., "Analysis of Ultrasonic Absorption Measurements in Liquids at High Pressures", High Pressure Laboratory (Harvard University), TR-4 (1967).

32. Papadakis, E. P., "Correction for Diffraction Losses in the Ultrasonic Field of a Piston Source", JASA 31, 150 (1959).

33. Velds, C. A., Los, J., DeVries, A. E., "Thermal Diffusion at Moderate Pressures in He-CO_2 Mixtures", Physica 35, 417 (1967).

34. Hilsenrath, J., Beckett, C. W., Benedict, W. S., Fano, L., Hoge, H. J., Masi, J. F., Nuttall, R. L., Touloukian, Y. S., and Woolley, H. W., Tables of Thermodynamic and Transport Properties of Air, Argon, Carbon Dioxide, Carbon Monoxide, Hydrogen, Nitrogen, and Steam, Pergamon Press, New York (1960).

REFERENCES (cont' d)

35. Brewer, J., "Determination of Mixed Viral Coefficients", Midwest Research Institute (AFOSR, Final Technical Report) (1965) AD 628 889.

36. Oertel, H., "High Speed Photography of Hypersonic Phenomena by a Schlieren Interferometric Method", Fifth International Congress on High Speed Photography, Washington, D. C. (1960).

37. Smeets, G., "Determination of Hot Gas Thermal Conductivity By Shock Tube Experiments", Proc. of the 5th International Shock Tube Symposium, 28-30, April 1965, AD 484 600.

38. Carey, C., Carnevale, E. H., Marshall, T., "Experimental Determination of the Transport Properties of Gases, Part II Heat Transfer and Ultrasonic Measurements", AFML-TR-65-141 (Wright-Patterson Air Force Base, Ohio, 1966). (See also Part I, 1965).

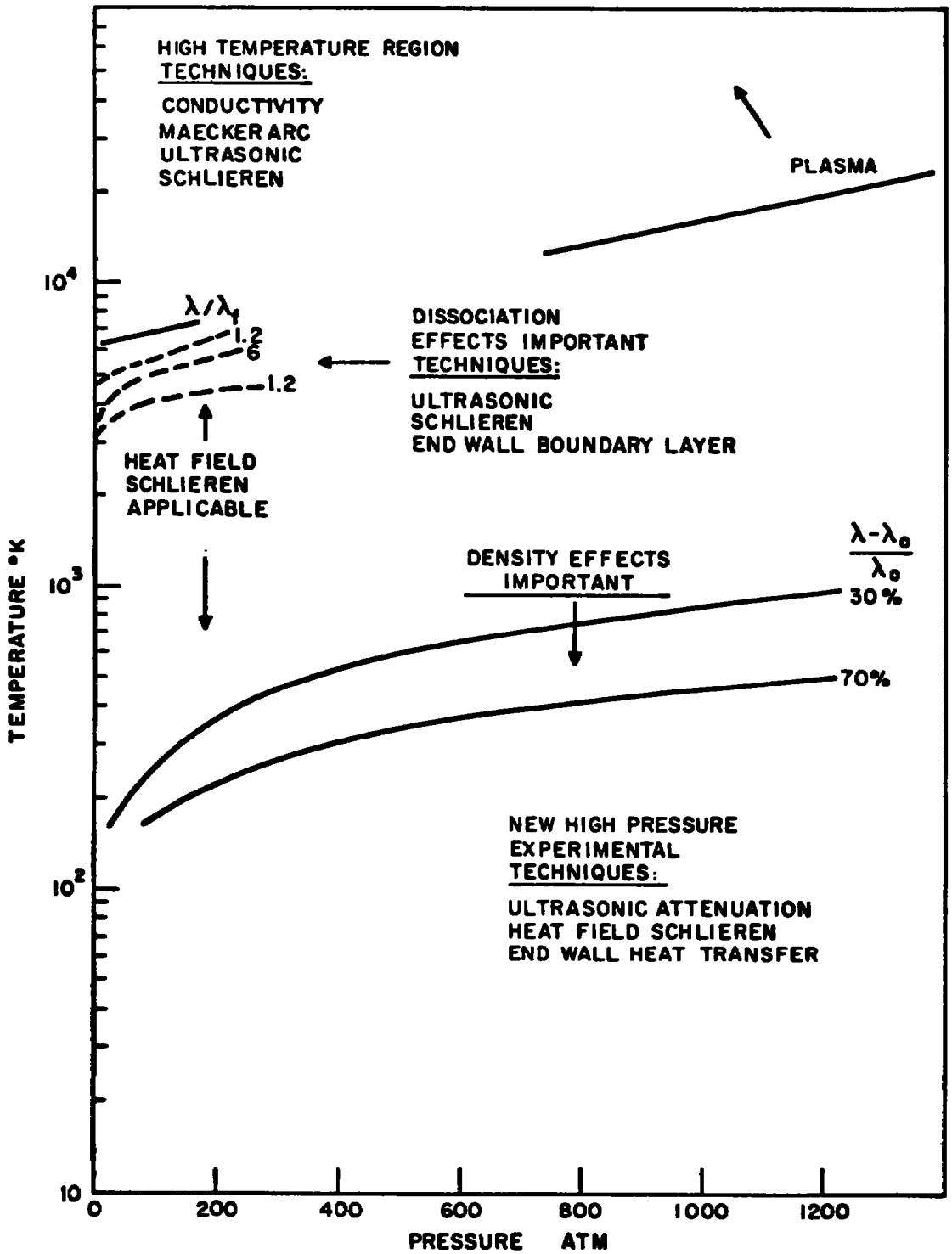

FIG. 1: PRESSURE-TEMPERATURE EFFECTS ON TRANSPORT PROPERTIES

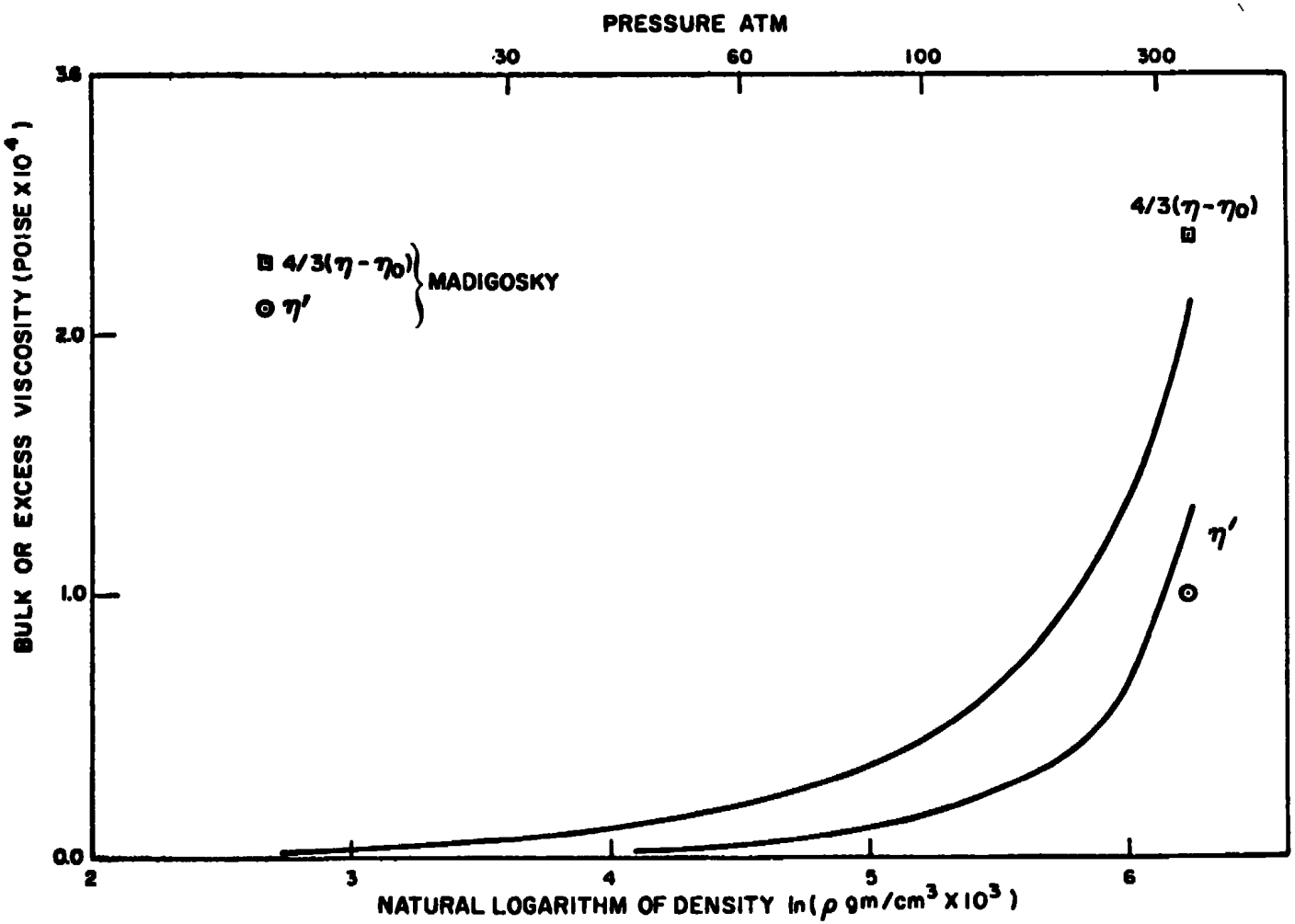

FIG. 2: CONTRIBUTION OF EXCESS VISCOSITY AND BULK VISCOSITY TERMS TO SOUND ABSORPTION IN ARGON

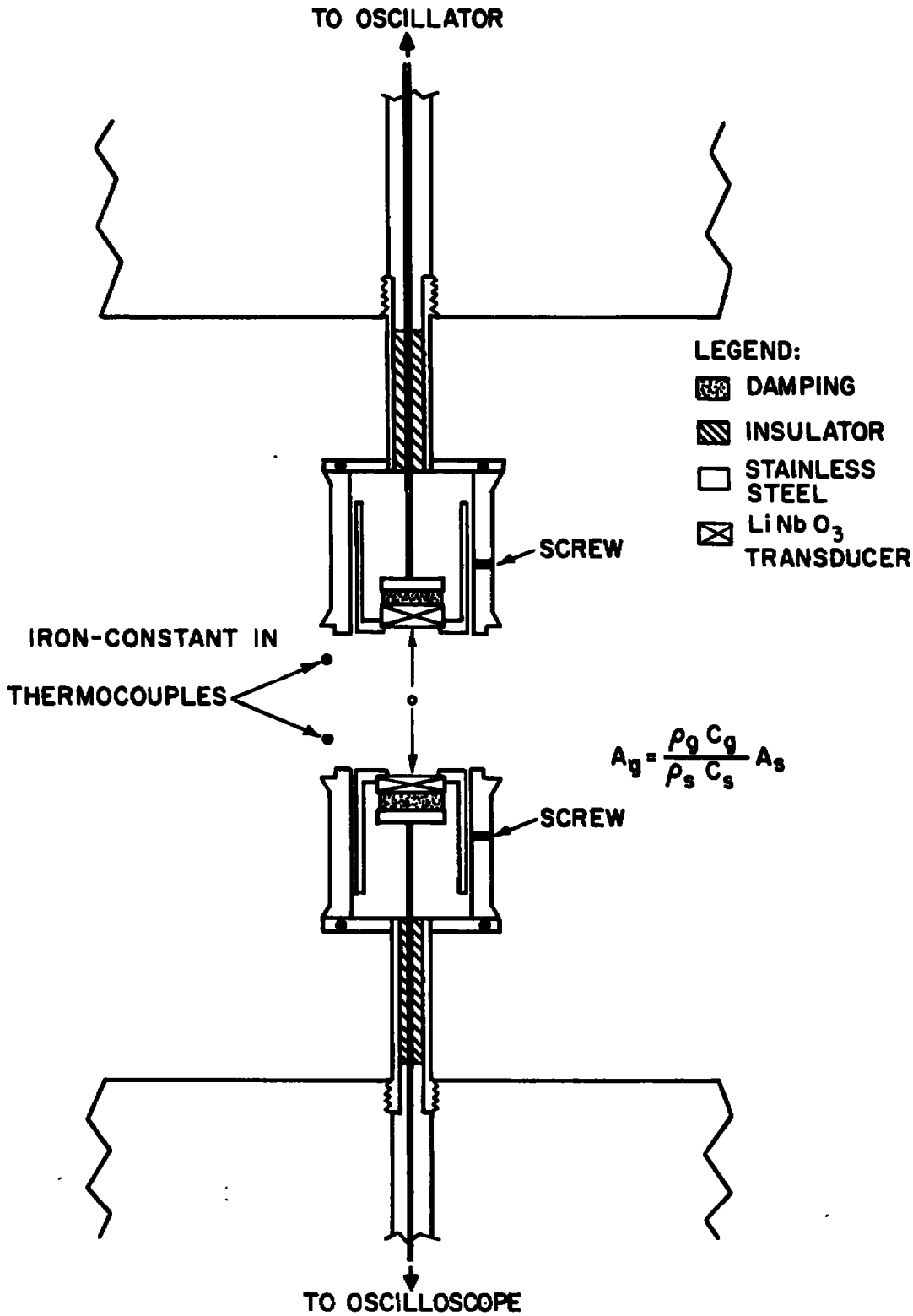

FIG. 3: HIGH PRESSURE ULTRASONIC PROBES

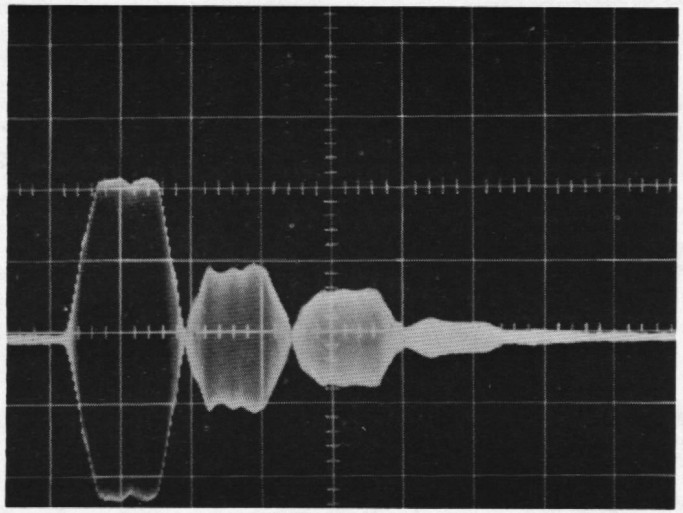

1.76 cm (probe separation)

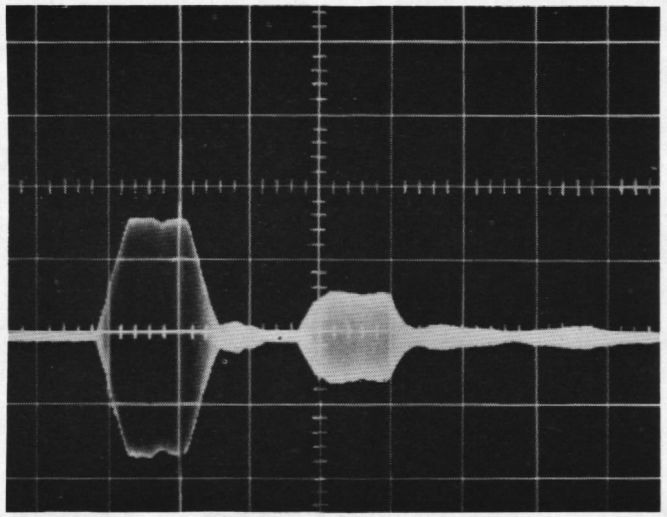

2.73 cm

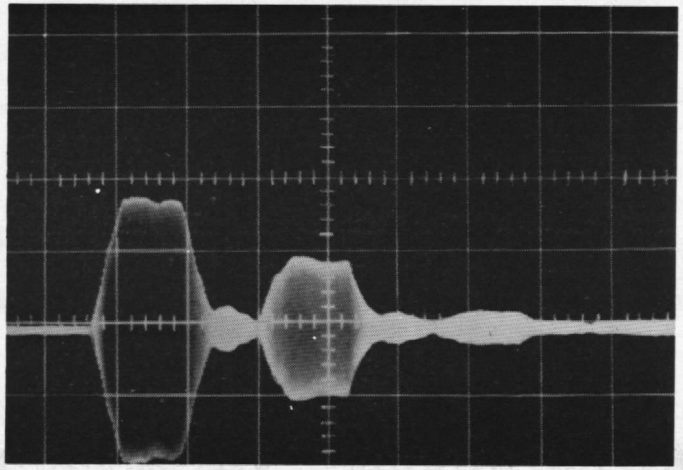

2.44 cm

50 μ sec/cm
1 mv/cm

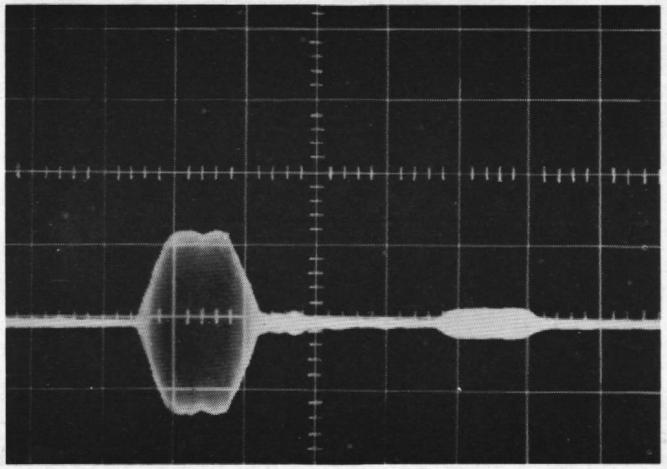

3.96 cm

Fig. 4. Through transmission multiple echo pulses in air

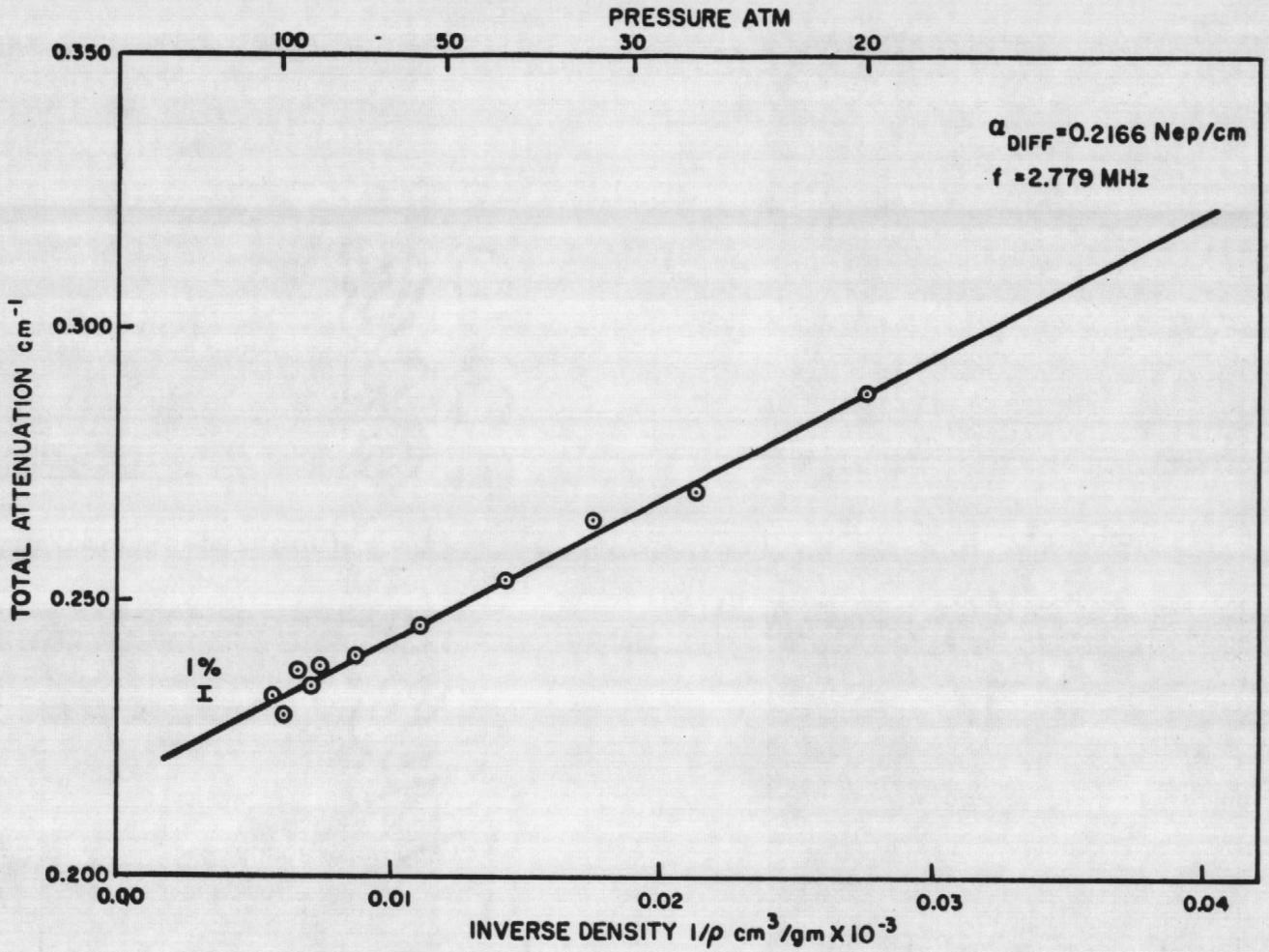

FIG. 5: TOTAL ABSORPTION IN ARGON

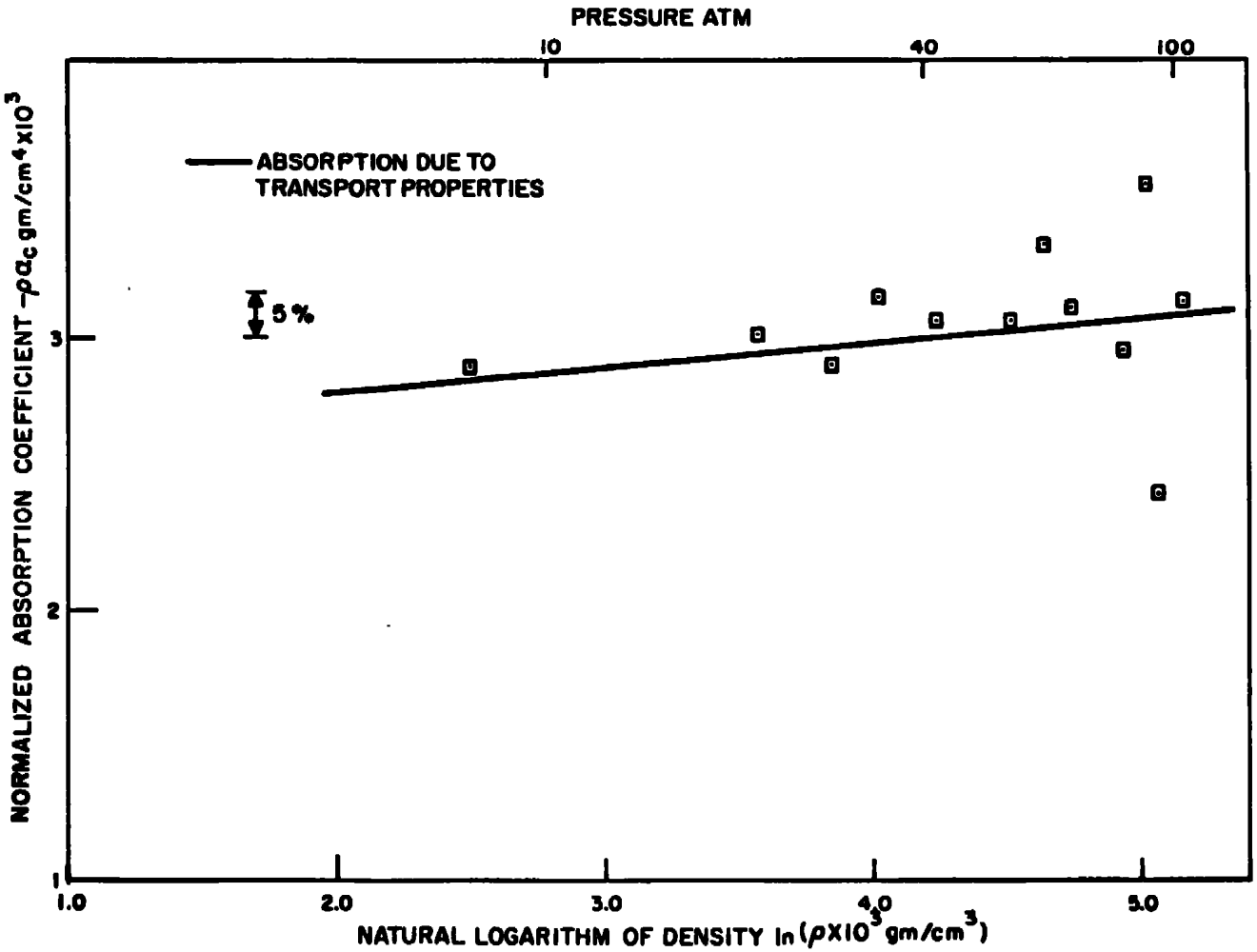

FIG. 6: ABSORPTION VS. DENSITY ARGON

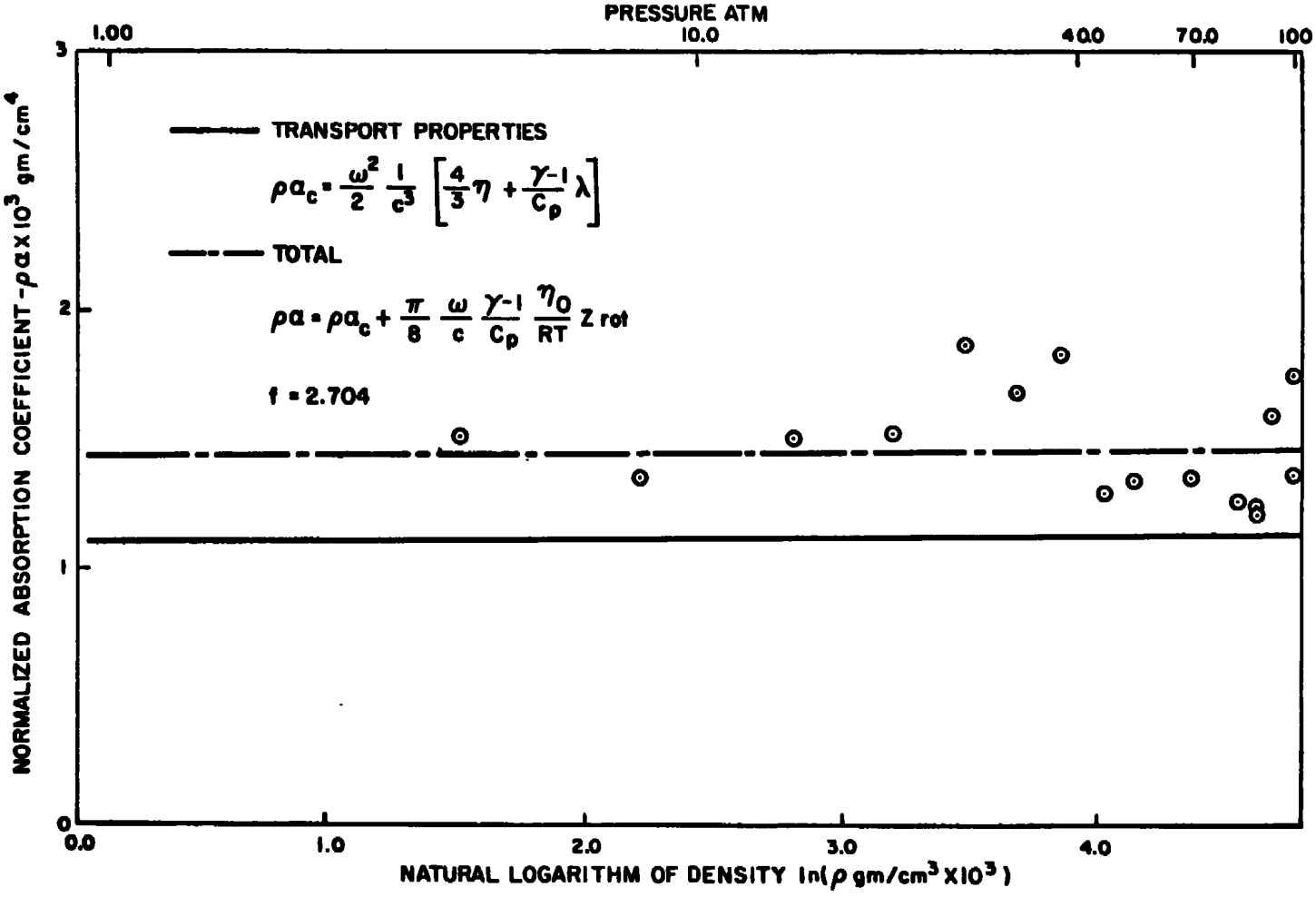

FIG. 7: ABSORPTION VS. DENSITY IN NITROGEN

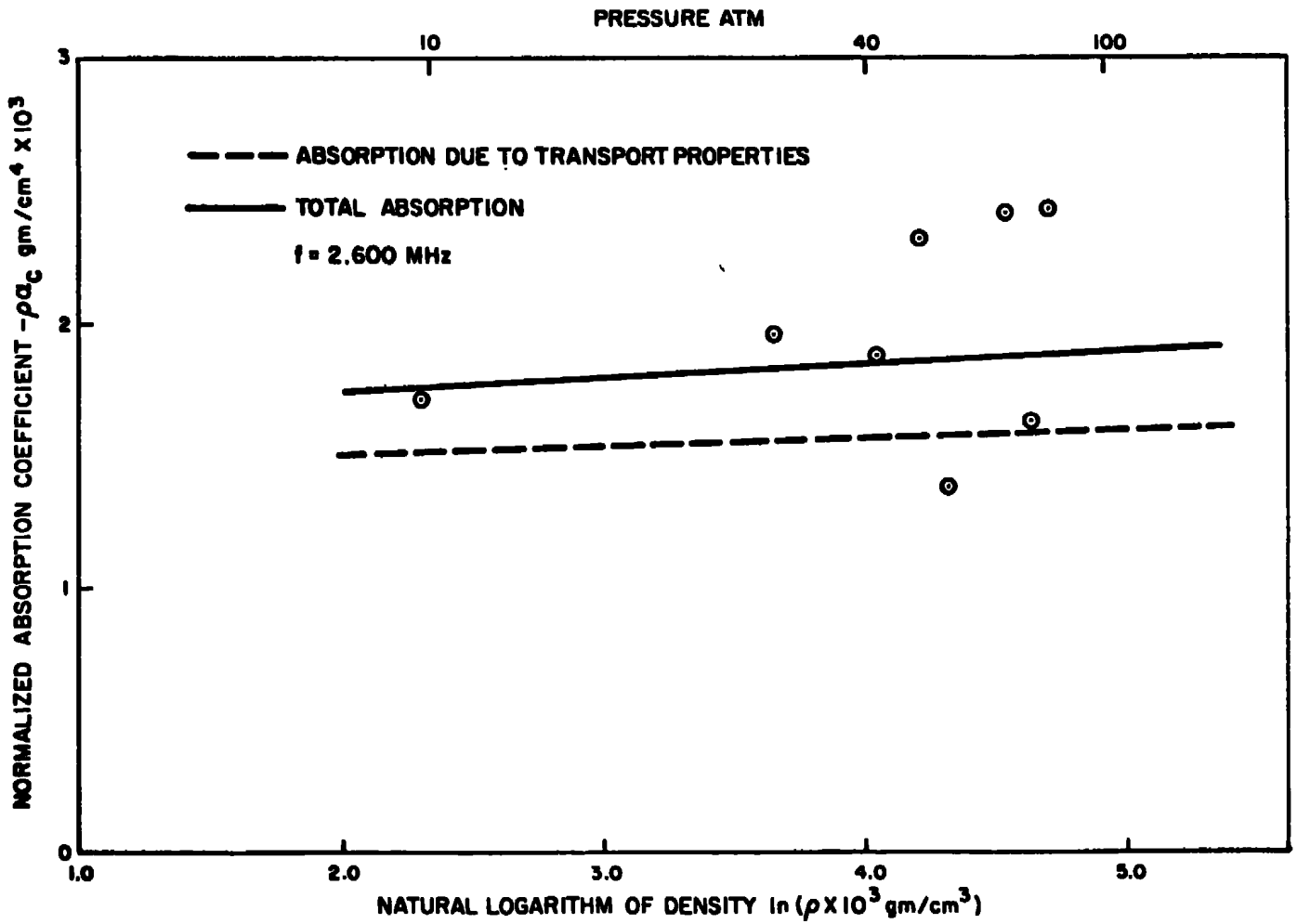

FIG. 8: ABSORPTION VS. DENSITY 50% ARGON-50% NITROGEN

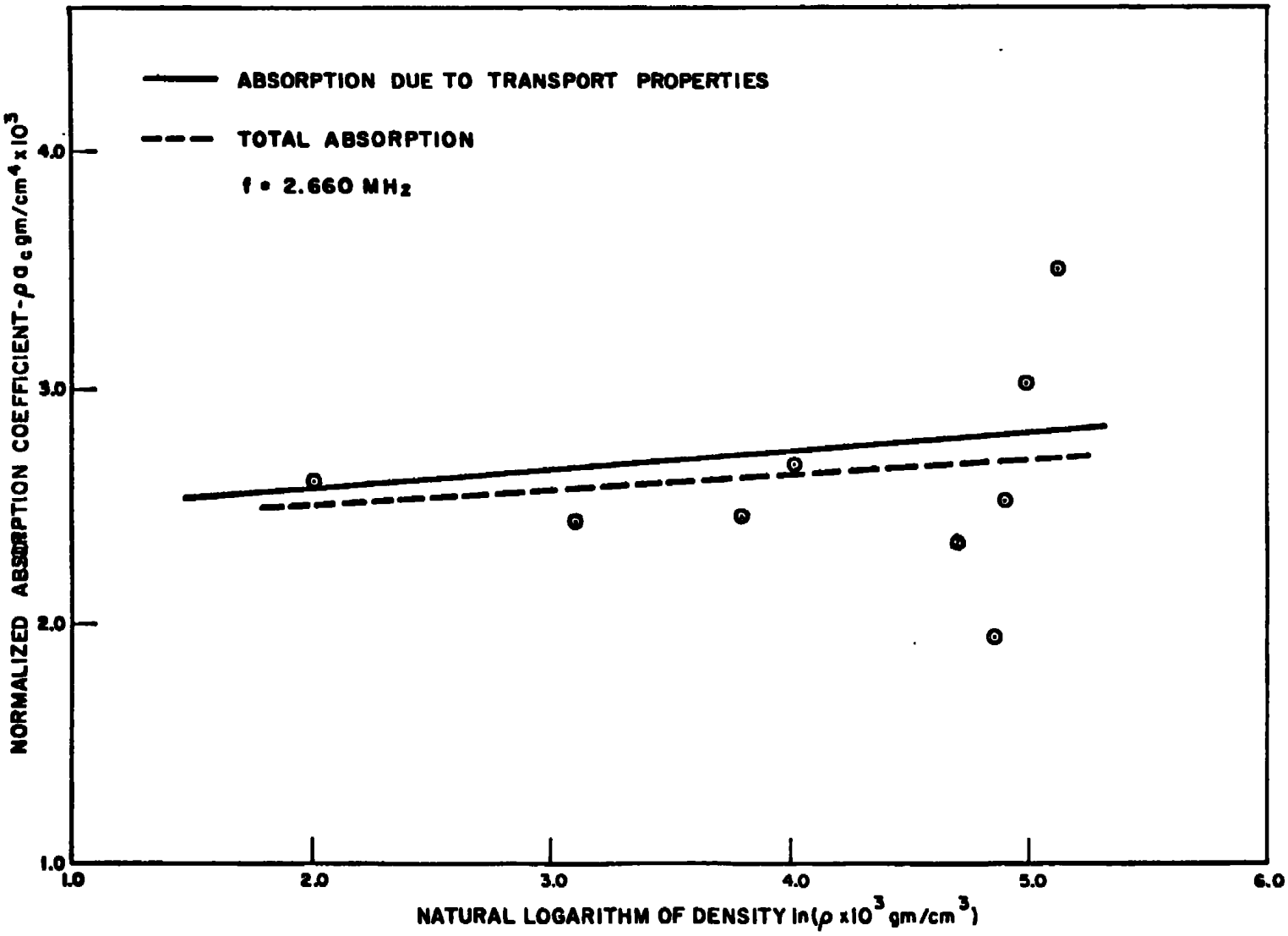

FIG. 9: ABSORPTION DENSITY 10% ARGON – 90% NITROGEN

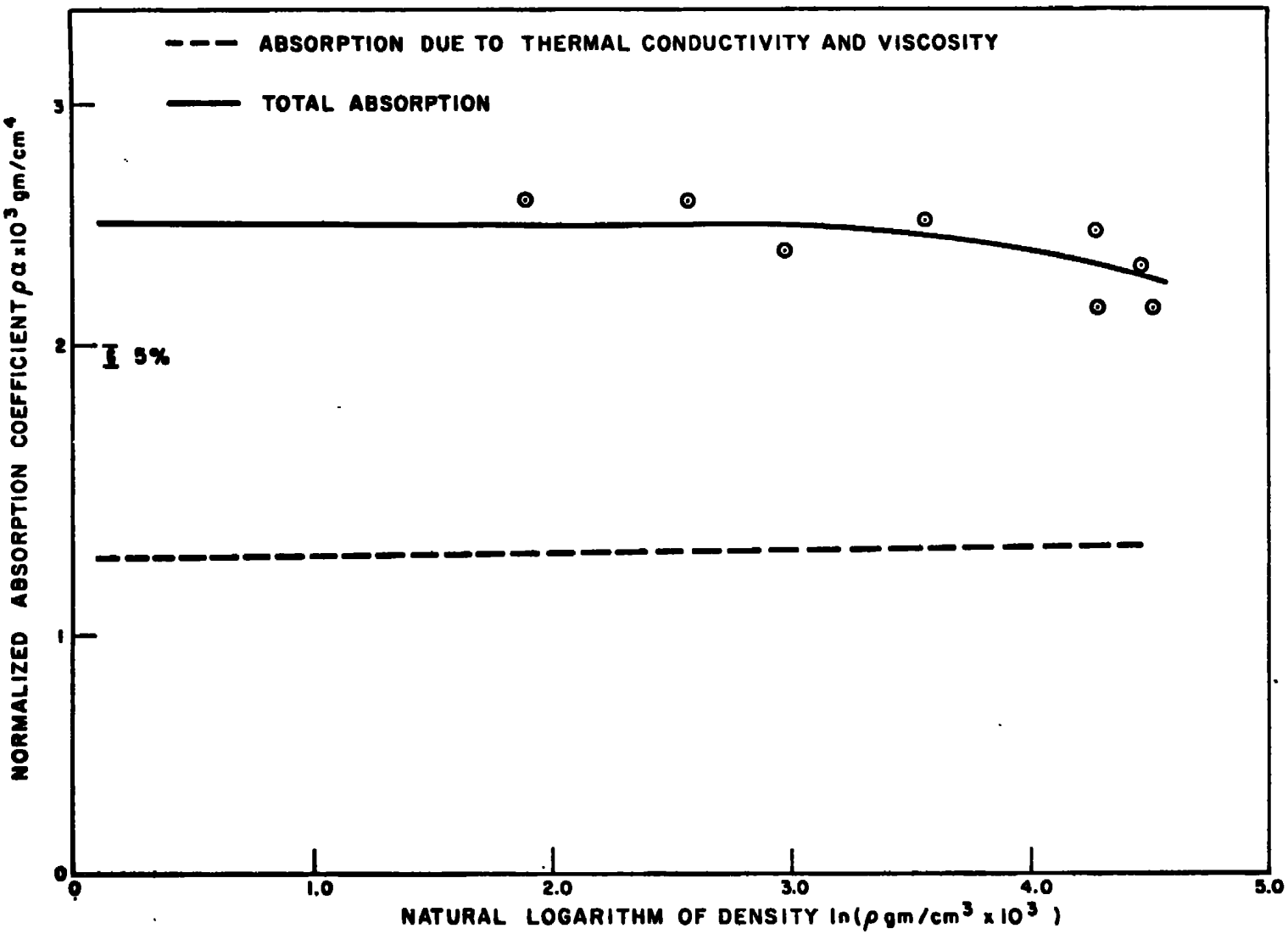

FIG. 10: ABSORPTION VS. DENSITY - 52.6 ARGON - 47.4 HELIUM

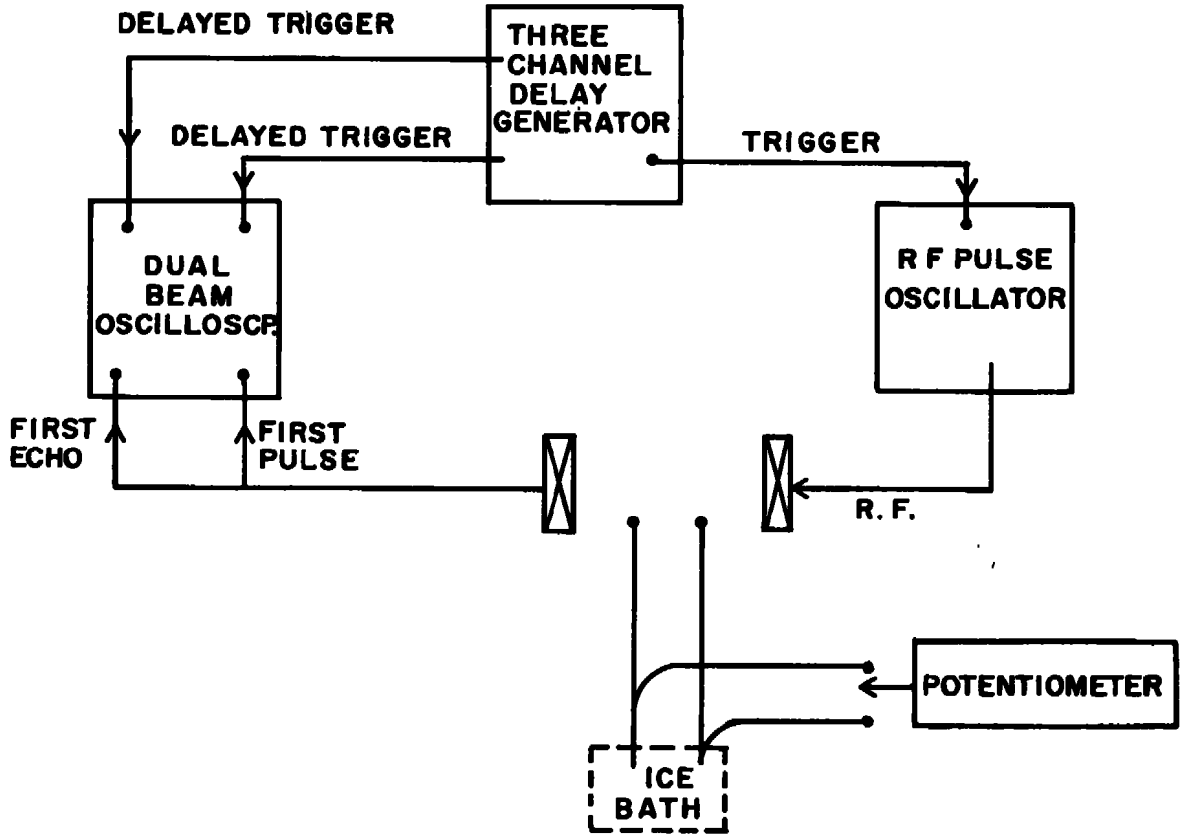

FIG. 11: ELECTRONICS FOR HIGH PRESSURE SOUND ABSORPTION AND VELOCITY MEASUREMENTS

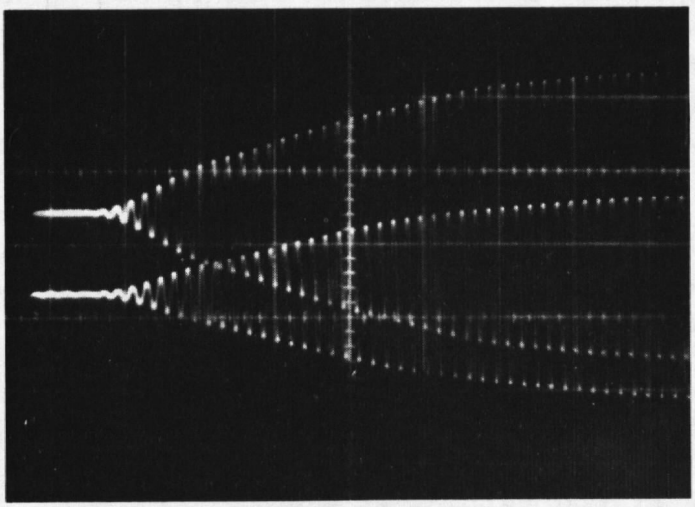

Upper Trace 1 V/cm
Lower Trace 0.5 V/cm
2 μ sec/cm
Argon 81.7 atm

Fig. 12. The first pulse and first echo used for absorption and velocity measurements.

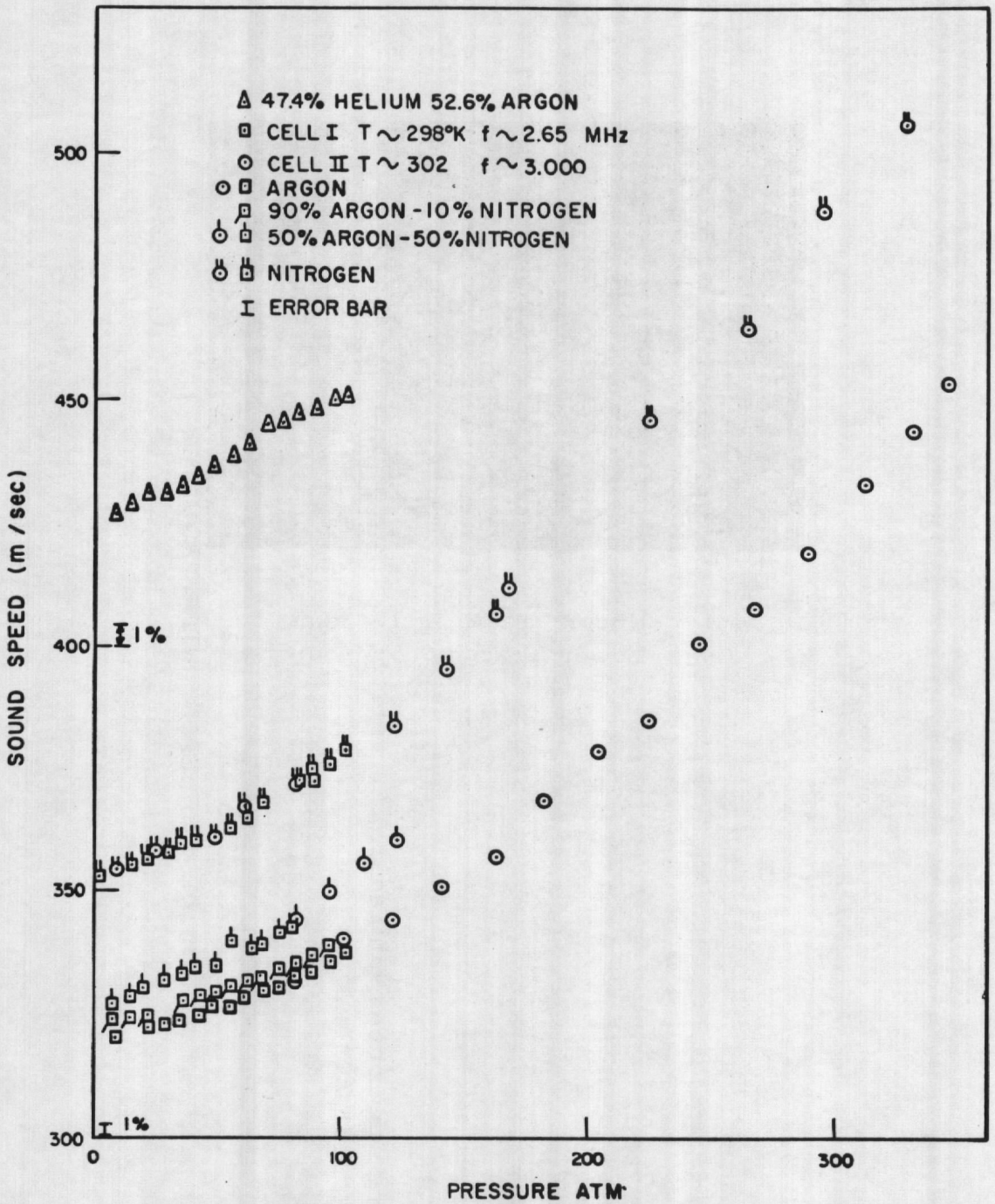

FIG. 13: SOUND SPEED VS. PRESSURE IN THE NITROGEN - ARGON SYSTEM AND A 47.4% HELIUM - 52.6% ARGON MIXTURE

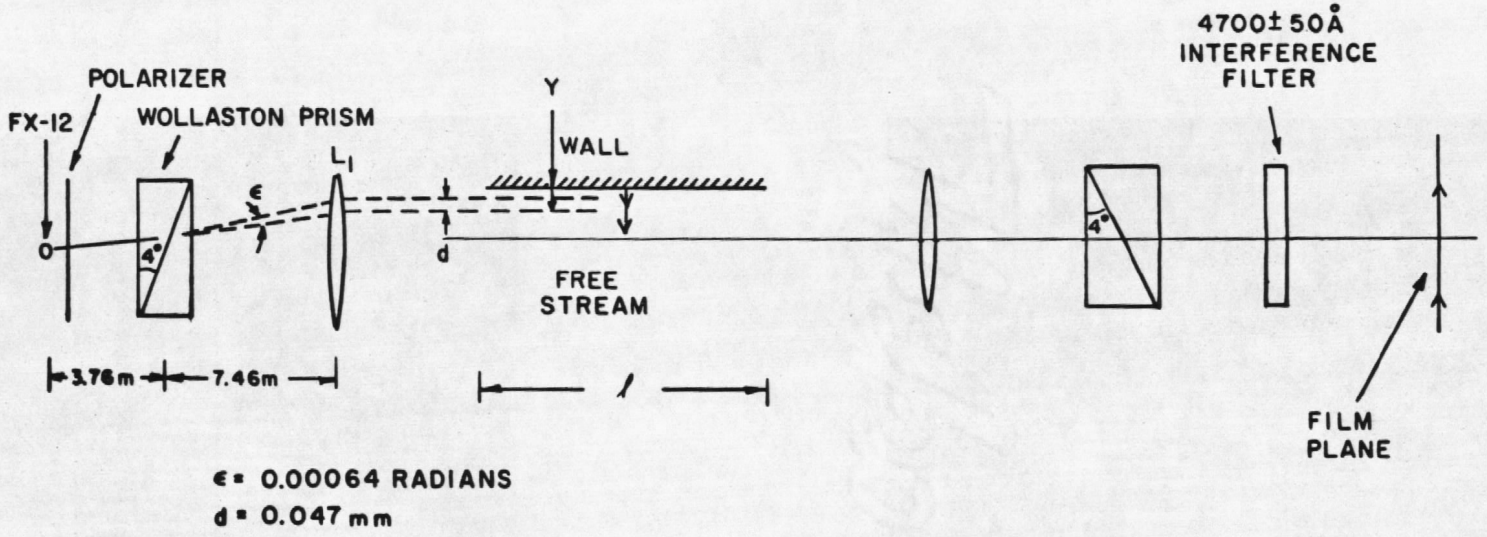

FIG. 14: SCHLIEREN INTERFEROMETER

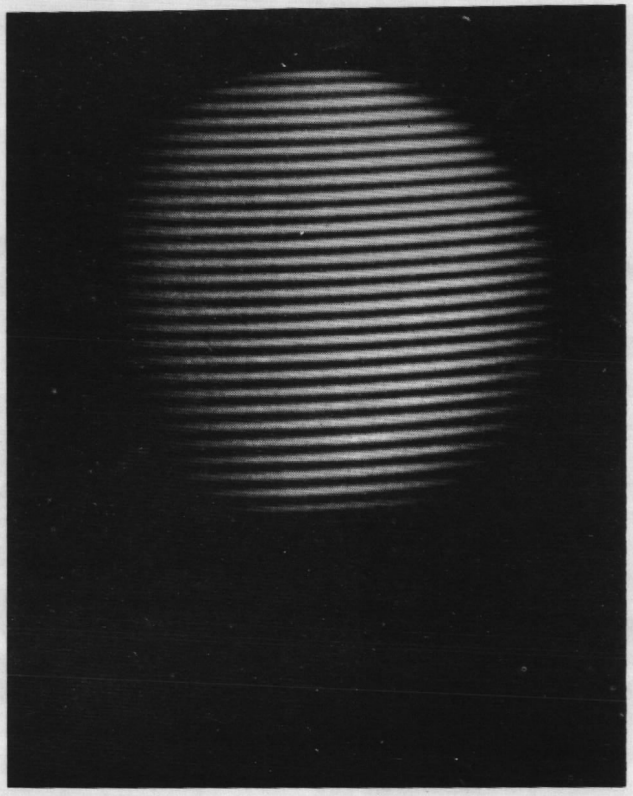

100 Å filter

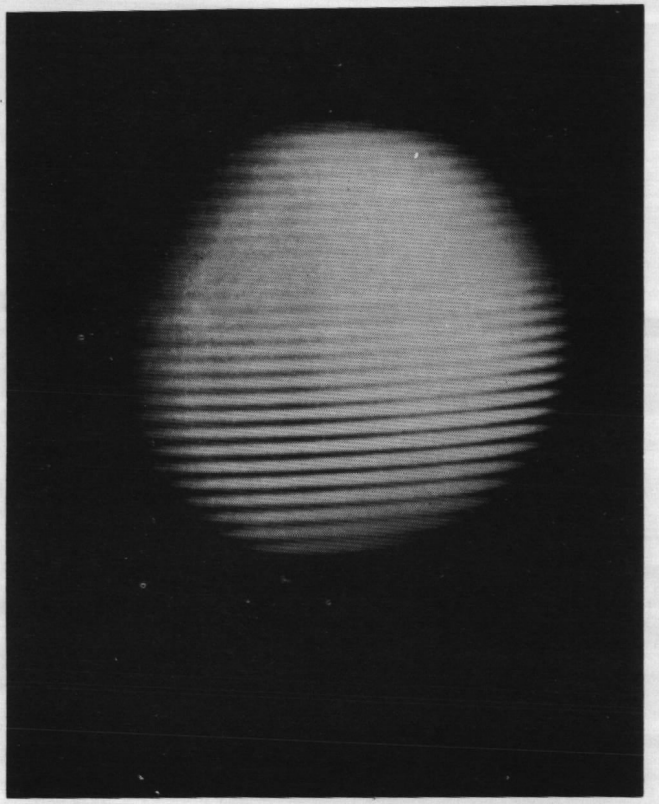

500 Å filter

Fig. 15. Effect of monochromaticity on the schlieren interferometer fringes

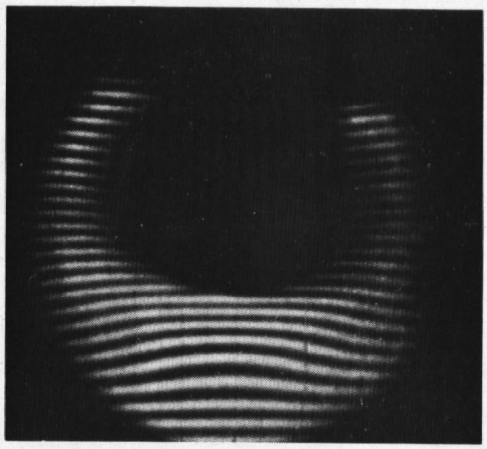

Vertical gradients $T_w = 900^{\circ}C$

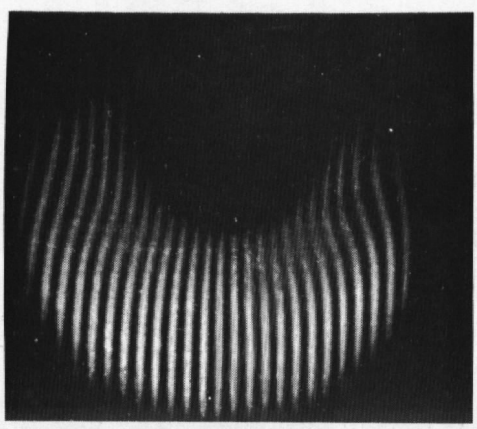

Horizontal gradients $T_w = 900^{\circ}C$

Fig. 16. Temperature field of a horizontal cylinder in free convection. (x 5)

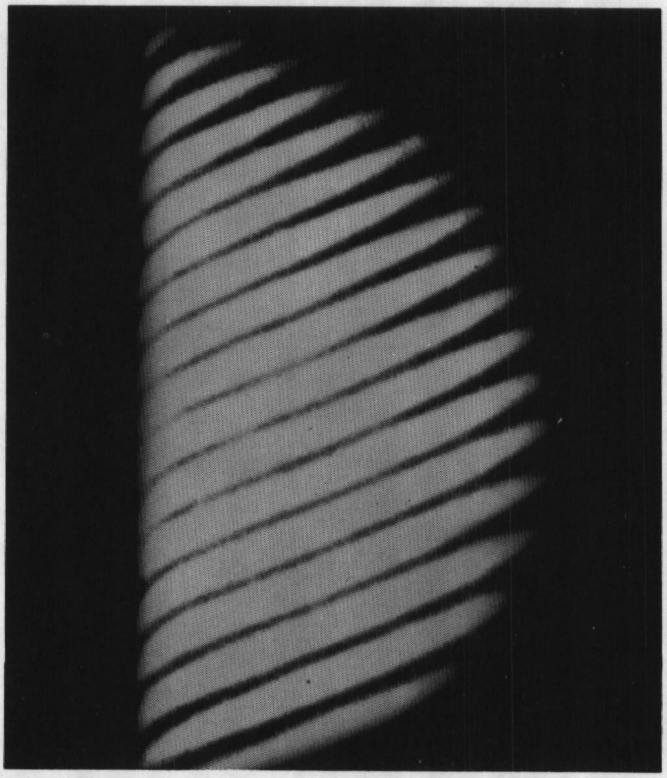

Fringe Field (x 2)

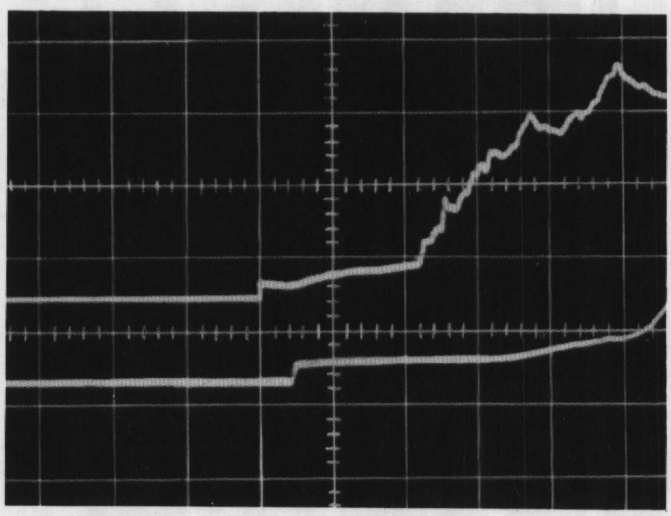

Heat Transfer Trace
200 μ sec/cm

Fig. 17. End wall boundary layer fringes and heat transfer gauge response

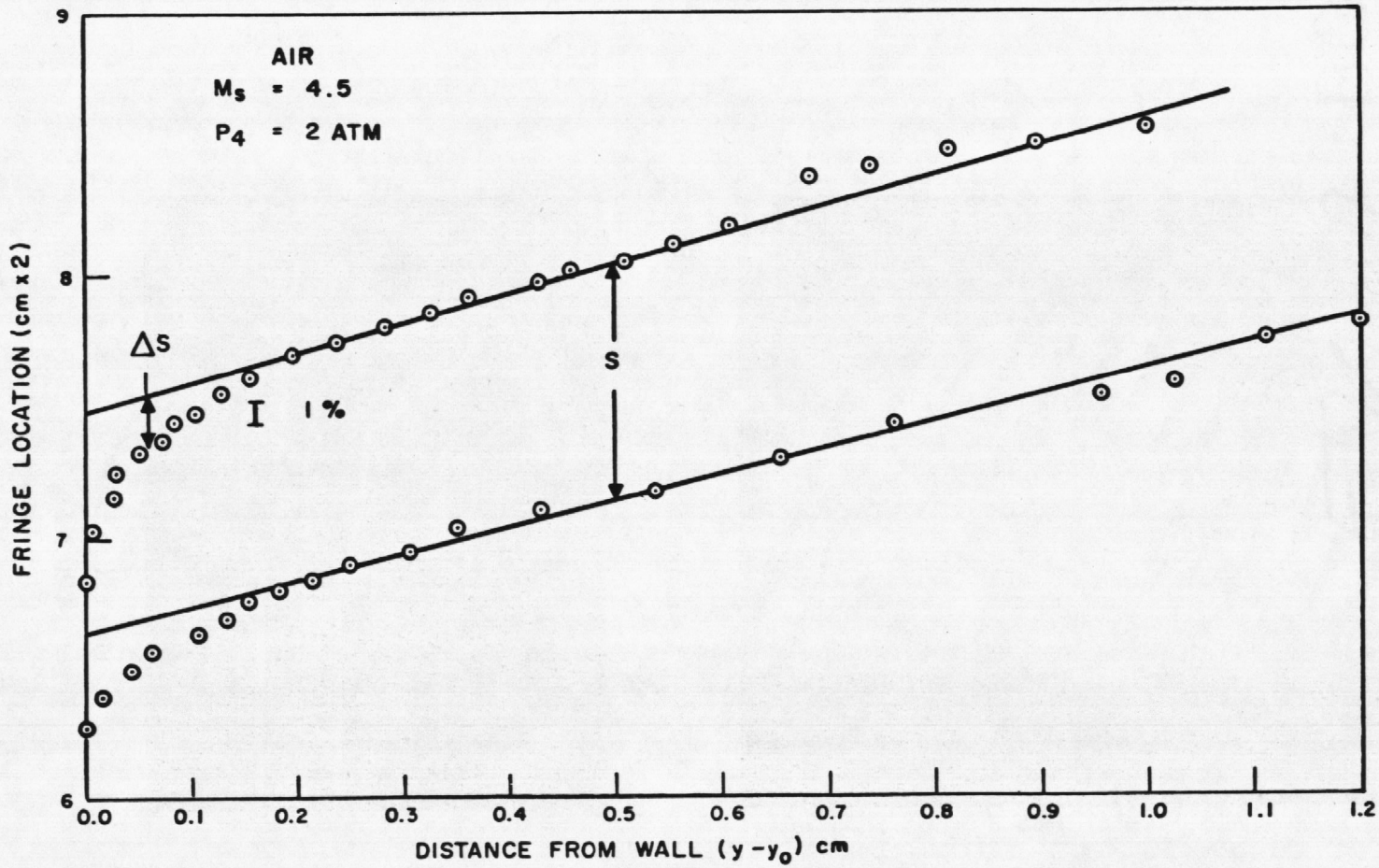

FIG. 18: FRINGE FIELD OF END WALL BOUNDARY LAYER

UNCLASSIFIED
Security Classification

DOCUMENT CONTROL DATA - R & D

(Security classification of title, body of abstract and indexing annotation must be entered when the overall report is classified)

1 ORIGINATING ACTIVITY *(Corporate author)*
Panametrics, Inc.
221 Crescent Street
Waltham, Massachusetts 02154

2a. REPORT SECURITY CLASSIFICATION
UNCLASSIFIED

2b. GROUP
N/A

3 REPORT TITLE
EXPERIMENTAL DETERMINATION OF GAS PROPERTIES AT HIGH TEMPERATURES AND/OR PRESSURES

4 DESCRIPTIVE NOTES *(Type of report and inclusive dates)*
September 1967 to October 1968 - Final Report

5. AUTHOR(S) *(First name, middle initial, last name)*
C. Carey, E. H. Carnevale, S. Uva, and T. Marshall

6. REPORT DATE	7a. TOTAL NO. OF PAGES	7b. NO. OF REFS
March 1969	59	38

8a. CONTRACT OR GRANT NO	9a. ORIGINATOR'S REPORT NUMBER(S)
AF 40(600)-1191	AEDC-TR-69-78
b. PROJECT NO: 8951	
c. Program Element 61102F	9b. OTHER REPORT NO(S) *(Any other numbers that may be assigned this report)*
d. Task 02	N/A

10 DISTRIBUTION STATEMENT
This document has been approved for public release and sale; its distribution is unlimited.

11 SUPPLEMENTARY NOTES	12. SPONSORING MILITARY ACTIVITY
Available in DDC	Arnold Engineering Development Center, Air Force Systems Command, Arnold Air Force Station, Tenn.

13 ABSTRACT

The problem of extending transport property measurements to conditions of high pressure $p < 10^4$ atm and temperature $T < 20{,}000^{\circ}K$ beyond the range of conventional techniques is summarized. The advantages of unconventional techniques over conventional transport property measurement techniques in regions where they overlap are presented for application at extreme pressure-temperature conditions. The application of ultrasonic absorption and sound speed to the determination of thermodynamic and transport properties at high pressures is discussed. Measurements are presented at $300^{\circ}K$ and pressures up to 100 atm in the argon-nitrogen and helium-argon systems. The schlieren differential interferometer is applied to thermal conductivity measurements at high pressures and/or temperatures. Some thermal conductivity measurements in nitrogen and air are reported at temperatures between 2000 and $5000^{\circ}K$.

DD FORM 1 NOV 65 1473

UNCLASSIFIED
Security Classification

14 KEY WORDS	LINK A		LINK B		LINK C	
	ROLE	WT	ROLE	WT	ROLE	WT
gases, properties of						
viscosity						
thermal conductivity						
kinetic theory						
diffusion						
transport properties						